

Adaptive Batching for Gaussian Process Surrogates with Application in Noisy Level Set Estimation

Xiong Lyu *

Department of Statistics and Applied Probability, University of California, Santa Barbara
and

Michael Ludkovski

Department of Statistics and Applied Probability, University of California, Santa Barbara

May 16, 2022

Abstract

We develop adaptive replicated designs for Gaussian process metamodels of stochastic experiments. Adaptive batching is a natural extension of sequential design heuristics with the benefit of replication growing as response features are learned, inputs concentrate, and the metamodeling overhead rises. Motivated by the problem of learning the level set of the mean simulator response we develop four novel schemes: Multi-Level Batching (MLB), Ratchet Batching (RB), Adaptive Batched Stepwise Uncertainty Reduction (ABSUR), Adaptive Design with Stepwise Allocation (ADSA) and Deterministic Design with Stepwise Allocation (DDSA). Our algorithms simultaneously (MLB, RB and ABSUR) or sequentially (ADSA and DDSA) determine the sequential design inputs and the respective number of replicates. Illustrations using synthetic examples and an application in quantitative finance (Bermudan option pricing via Regression Monte Carlo) show that adaptive batching brings significant computational speed-ups with minimal loss of modeling fidelity.

Keywords: metamodeling, stochastic simulators, replicated design of experiments

1 Introduction

Metamodels offer a cheap statistical representation of complex and/or expensive stochastic simulators that arise in applications ranging from engineering to environmental science and finance [Santner et al., 2013]. Gaussian process (GP) frameworks have emerged as the leading family of metamodels thanks to their flexibility, analytical tractability and superior empirical performance. However, for GP metamodels to be fast, it is imperative to keep the respective design size $|\mathcal{A}|$ manageable. In particular, unless the simulator is truly expensive or the input domain is vast, the typical recommendation is to restrict to hundreds of inputs, $|\mathcal{A}| \ll 10^3$. This creates a major tension as frequently the stochastic simulator has low signal-to-noise ratio or a complex noise structure. A prototypical example is where the simulator $Y(x) = F(X_{[0, \Delta t]})|_{X_0=x}$ involves functionals of a continuous-time Markov chain or stochastic differential equation solution (X_t) , whereby the stochasticity tends to dominate the trend/drift term for short Δt , and moreover simulation noise is non-Gaussian and state-dependent (heteroskedastic).

*Both authors are partially supported by NSF DMS-1521743. ML is additionally supported by NSF DMS-1821240

A natural solution is to employ *batching*, known in the stochastic simulation community as nested Monte Carlo. Re-using the same input to generate multiple outputs allows for a Law of Large Numbers (LLN) averaging which can be analytically combined with the GP predictive equations to keep the computational complexity as a function of k (number of unique inputs) rather than of the capital- N (number of simulator calls). The seminal technique of *stochastic kriging* [Ankenman et al., 2010] shows that these computational savings are exact assuming the GP hyperparameters, in particular the noise variance τ^2 , are known. Such batching becomes critical in the use of GP models in our motivating application of solving optimal stopping problems via Regression Monte Carlo, where tens of thousands of simulations are called for.

In the classical setup, the metamodeling objective is to learn the mean response over the entire domain [Koehler et al., 1998, Le Gratiet and Garnier, 2015, Chen and Zhou, 2017], whereby, modulo heteroskedastic noise, one expects to utilize the same batching level across all inputs, i.e. splitting the total budget $N = k \times r$ into k batches of r replicates at locations $\bar{x}_1, \dots, \bar{x}_k$. See Ankenman et al. [2010] for a discussion of how to pick k for a given budget N , as well as some proposals for handling non-constant $\tau^2(x)$. We are interested in more targeted objectives, where the picture is much less clear. As two canonical examples we recall Bayesian Optimization (finding the maximum mean response) and Level Set Estimation (determining the input sub-domain where the mean response exceeds a given threshold). In both settings GP metamodels have been shown to especially shine, not least because they organically match the sequential adaptive designs typically utilized; the respective Expected Improvement schemes form a major feature of the GP ecosystem. Since these objectives imply preferentially sampling a small portion of the input space—the neighborhood of the maximum, or the neighborhood of the desired contour—the exploration-exploitation paradigm leads to increasingly concentrated designs. Such concentration suggests to adaptively determine the amount of batching. Intuitively, replication should be low for more exploratory sites and should rise in the neighborhood of interest, where we replicate to achieve computational savings. Indeed, the intrinsic cost of replication is linked to the variability of the response at the respective inputs, which will be minimal if the inputs are very close together. From a different perspective, replication trades off costly, precise outputs (large r) vis-a-vis cheap outputs with low signal-to-noise ratio (low r).

The above motivates *adaptively batched* designs, where r is input-dependent. While this idea was investigated for Bayesian Optimization [Klein et al., 2017, Poloczek et al., 2017] and for Integrated Mean Square Error (IMSE) minimization [Ankenman et al., 2010, Binois et al., 2018], neither of these fully reveal the underlying tension between exploration (replicate less, larger metamodel overhead) and exploitation (replicate more, generate computational savings). In this article we propose several schemes that explicitly focus on this issue. To evaluate them we concentrate on the problem of level set estimation where the contour is adaptively learned through the sequential design but retains a spatial structure (unlike Bayesian Optimization where convergence to the single input yielding the global maximum is desired). Consequently, we expect a complex interaction between the selection of inputs and the respective replication amounts. In this context, our main contribution is to extend the paradigm of Expected Improvement to include sequential selection of both the input locations x_n and the replication counts r_n . We benchmark the proposed algorithms and show that they provide significant savings compared to the naive fixed-batching approach. In particular, we are able to obtain schemes that reduce $N \simeq 10^5$ simulations to efficient replicated designs of just a few hundred unique inputs.

Beyond benchmarking the developed algorithms on several synthetic examples, we also implement them for the motivating application of valuation of Bermudan options. In the latter context, the Regression Monte Carlo (RMC) paradigm is used to provide a simulation-based algorithm that hinges on recursive estimation of certain level sets that correspond to the so-called stopping bound-

aries. Building upon the successful use of GP surrogates for RMC [Ludkovski, 2018, Lyu et al., 2018], we demonstrate that adaptive batching significantly speeds up this approach, making it more scalable and efficient. In particular while in [Ludkovski, 2018] sequential design was typically too slow to be useful, adaptively batched models beat basic implementation on both speed and memory requirements. We note that there are other important applications of level set estimation, from quantifying the reliability of a system or its failure probability [Bect et al., 2012], to ranking pay-offs from several available actions in dynamic programming [Hu and Ludkovski, 2017].

The rest of the paper is organized as follows. Section 2 formalizes the GP model and the contour-learning objective. Section 3 develops heuristics for sequential designs that jointly optimize over the new input and replication level. Section 4 takes a different tack and explores dynamic replication through allocating new simulations to existing inputs. Section 5 benchmarks the proposed schemes on three synthetic case studies and Section 6 on two more examples from Bermudan option pricing. Section 7 concludes.

2 Statistical Model

Consider a latent $f : D \rightarrow \mathbb{R}$ which is a continuous function over a d -dimensional input space $D \subseteq \mathbb{R}^d$. We wish to identify the contour ∂S , where, without loss of generality, S is the zero level set

$$S = \{x \in D : f(x) \geq 0\}. \quad (1)$$

Thus, our metamodeling objective is equivalent to learning the sign of $f(x)$ for any $x \in D$. For any $x_i \in D$, we have access to a simulator $Y(x_i)$ that generates noisy outputs of $f(x_i)$:

$$Y(x_i) = f(x_i) + \epsilon_i, \quad (2)$$

where ϵ_i 's are realizations of independent, mean zero random variables with variance τ^2 . To describe replicated inputs, let \bar{x}_i , $i = 1, \dots, k$ denote the unique inputs, and $y_i^{(j)}$ be the j^{th} output of $r_i \geq 1$ replicates observed at \bar{x}_i . Let $\bar{\mathbf{y}}_{1:k} = \{\bar{y}_i, 1 \leq i \leq k\}$ store averages over replicates, $\bar{y}_i := \frac{1}{r_i} \sum_{j=1}^{r_i} y_i^{(j)}$.

The inference of ∂S proceeds by building a metamodel \hat{f} , which induces \hat{S} , and evaluating its *error rate* \mathcal{ER} , i.e. the integral over the symmetric difference between \hat{S} and true S weighted by a given measure $\mu(\cdot)$:

$$\mathcal{ER}(S, \hat{S}) = \int_{x \in D} \mathbb{I}(\text{sign } \hat{f}(x) \neq \text{sign } f(x)) \mu(dx) = \mu(S \Delta \hat{S}), \quad (3)$$

where $S \Delta \hat{S} := (S \cap \hat{S}^c) \cup (S^c \cap \hat{S})$.

Reconstructing S via a metamodel can be divided into two aspects: the construction of the response model $x \mapsto Y(x)$, and the development of the design of experiments (DoE) for efficiently selecting the inputs $\bar{x}_1, \bar{x}_2, \dots$. To account for the second aspect, we use n to denote the rounds of sequential DoE, k_n to denote the number of unique inputs \bar{x} 's sampled by step n and $N_n = \sum_{i=1}^{k_n} r_i^{(n)}$ the respective number of simulator calls made. The superscript on r_i allows the replicate counts to evolve over n as well, see Section 4. The metamodel training set by step n consists of $\mathcal{A}_n = \{(\bar{x}_i, r_i^{(n)}, \bar{y}_i), 1 \leq i \leq k_n\}$.

The Gaussian process paradigm treats f as a random function whose posterior distribution is determined from its prior and the training set(s) \mathcal{A}_n . We view $f(\cdot) \sim GP(m(\cdot), K(\cdot, \cdot))$ as a realization of a Gaussian process specified by its mean function $m(x) := \mathbb{E}[f(x)]$ and covariance

function $K(x, x') := \mathbb{E}[(f(x) - m(x))(f(x') - m(x'))]$. The noise distribution is $\epsilon \sim \mathcal{N}(0, \tau^2)$; for simplicity we take $m(x) = 0$. The conditional distribution $f|\mathcal{A}_n$ is another Gaussian process, with posterior mean $\hat{f}^{(n)}(x_*)$ and covariance $v^{(n)}(x_*, x'_*)$ at arbitrary inputs x_*, x'_* given by

$$\hat{f}^{(n)}(x_*) = \mathbf{k}(x_*)[\mathbf{K} + \tau^2\mathbf{R}^{(n)}]^{-1}\bar{\mathbf{y}}_{1:k_n}, \quad (4)$$

$$v^{(n)}(x_*, x'_*) = K(x_*, x'_*) - \mathbf{k}(x_*)[\mathbf{K} + \tau^2\mathbf{R}^{(n)}]^{-1}\mathbf{k}(x'_*)^T, \quad (5)$$

with the $1 \times k_n$ vector $\mathbf{k}(x_*) = K(x_*, \bar{\mathbf{x}}_{1:k_n})$, the $k_n \times k_n$ matrix \mathbf{K} given by $\mathbf{K}_{ij} = K(\bar{x}_i, \bar{x}_j)$, and the $k_n \times k_n$ diagonal matrix $\mathbf{R}^{(n)}$ given by $R_{ii}^{(n)} := \frac{1}{r_i^{(n)}}$. The posterior mean $\hat{f}^{(n)}(x_*)$ is treated as a point estimate of $f(x_*)$, and the posterior standard deviation $s^{(n)}(x_*) := \sqrt{v^{(n)}(x_*, x_*)}$ as the uncertainty of this surrogate.

3 Adaptive Designs

3.1 Level Set Estimation

An adaptive DoE approach is needed to select $\bar{x}_1, \bar{x}_2, \dots$ sequentially since the level-set S is defined in terms of the unknown f . The standard framework of DoE is to add new inputs one-by-one at each round, using an acquisition function $\mathcal{I}_n(x)$ to pick \bar{x}_{n+1} . The acquisition function quantifies the value of information from running a new simulation at x conditional on an existing training set \mathcal{A}_n , and picks \bar{x}_{n+1} as the myopic maximizer of \mathcal{I}_n :

$$\bar{x}_{n+1} = \arg \sup_{x \in D} \mathcal{I}_n(x). \quad (6)$$

Building upon the seminal Expected Improvement criterion [Jones et al., 1998], various level-set sampling criteria were proposed by Bichon et al. [2008], Picheny et al. [2010], Bect et al. [2012] and Ranjan et al. [2008]. Further instances of $\mathcal{I}(x)$ can be found in Chevalier et al. [2013, 2014a], Azzimonti et al. [2016, 2020], and Bolin and Lindgren [2015]. The basic idea in sequential level-set estimation is to assess the *information gain* from new simulations, targeting the learning of the contour. Most of the above criteria were originally proposed for deterministic experiments with no simulation noise, or cases with known τ^2 . We refer to Lyu et al. [2018] for a summary of level set estimation in stochastic experiments with heteroskedastic $\tau^2(x)$, which can be seen as the counterpart of the earlier study in Jalali et al. [2017] for Bayesian Optimization with stochastic simulators.

In this section we construct a sequential batched DoE to jointly select (\bar{x}_{n+1}, r_{n+1}) . At each DoE round we pick a *new* input \bar{x}_{n+1} and the associated replication amount r_{n+1} ; thus by round n there are n unique inputs. In our first proposal, we formulate this task within a multi-fidelity framework, which is now widely used in Bayesian Optimization [Kandasamy et al., 2016a,b, 2017, Poloczek et al., 2017]. Thanks to the LLN, we interpret r_n as *fidelity*: a small number of replicates is cheap but inaccurate; inputs with a large number of replicates are viewed as high-fidelity queries: expensive but accurate. Our interest is then to choose the fidelity level to query next, balancing the trade-off between accuracy and cost. As a second proposal, we relate replication to simulation and model fitting overhead costs, leading to maximization of the information gain $\mathcal{I}(x, r)$ per unit cost [Klein et al., 2017, McLeod et al., 2017].

Remark. Another meaning of batched DoE refers to selecting multiple new inputs \bar{x}_k in parallel, see Chevalier et al. [2014a]. In this article, batching always refers to using replicates; we add (at most) one new input at each DoE round.

To begin, we recall two existing acquisition functions well suited to our needs. The first one is Maximum Contour Uncertainty (MCU) [Lyu et al., 2018] which stems from the Upper Confidence Bound (UCB) strategies proposed by Srinivas et al. [2012] for Bayesian Optimization. MCU blends the minimization of $|\hat{f}^{(n)}(x)|$ (exploitation) with maximization of the posterior uncertainty $s^{(n)}(x)$ (exploration):

$$\mathcal{I}_n^{\text{MCU}}(x) := \left\{ -|\hat{f}^{(n)}(x)| + \rho^{(n)} s^{(n)}(x) \right\} \mu(x), \quad (7)$$

where $\gamma^{(n)}$ is a sequence of UCB weights. Thus, MCU targets inputs with high response uncertainty (large $s^{(n)}(x)$), and close to the contour $\partial\hat{S}$ (small $|\hat{f}^{(n)}(x)|$). See Lyu et al. [2018] on the choice of the UCB weight sequence $\rho^{(n)}$.

The alternative Contour Stepwise Uncertainty Reduction (cSUR) criterion focuses on quickly *reducing* the local empirical error E_n defined by

$$E_n(x) := \Phi\left(-\frac{|\hat{f}^{(n)}(x)|}{s^{(n)}(x)}\right). \quad (8)$$

We interpret $E_n(x)$ as the local probability of misclassification of $\{x \in S\}$, see Bichon et al. [2008], Echard et al. [2010], Lyu et al. [2018], Ranjan et al. [2008]. cSUR aims to select the input which produces the greatest reduction between the current $E_n(x)$ given \mathcal{A}_n and the expected $E_{n+1}(x)$ conditional on the one-step-ahead design, $\mathcal{A}_{n+1} = \mathcal{A}_n \cup (\bar{x}_{n+1}, r_{n+1}, \bar{y}_{n+1})$. To do so, cSUR ties the selection of \bar{x}_{n+1} to the look-ahead standard deviation $s^{(n+1)}(x, r)$ at x conditional on \mathcal{A}_n and sampling r times at x . The latter is proportional to the current standard deviation $s^{(n)}(x)$ with the proportionality factor linked to r [Chevalier et al., 2014b]:

$$\frac{s^{(n+1)}(x, r)^2}{s^{(n)}(x)^2} = \frac{\frac{\tau^2}{r}}{\frac{\tau^2}{r} + s^{(n)}(x)^2}, \quad (9)$$

since the replicated outputs $y_{n+1}^{(j)}$ are i.i.d.. Based on (9) and using the fact that $\mathbb{E}_{\bar{Y}(x)}[\hat{f}^{(n+1)}(x)] = \hat{f}^{(n)}(x)$, the cSUR metric approximates the effect of $\bar{Y}(x)$ on the look-ahead local empirical error $E_{n+1}(x)$:

$$\begin{aligned} \mathcal{I}_n^{\text{cSUR}}(x, r) &:= \left\{ \Phi\left(-\frac{|\hat{f}^{(n)}(x)|}{s^{(n)}(x)}\right) - \Phi\left(-\frac{|\hat{f}^{(n)}(x)|}{s^{(n+1)}(x, r)}\right) \right\} \mu(x) \\ &\simeq \left\{ E_n(x) - \mathbb{E}_{\bar{Y}(x)}[E_{n+1}(x)] \right\} \mu(x). \end{aligned} \quad (10)$$

We note that $\mathcal{I}_n^{\text{cSUR}}(x, r) = 0$ for $x \in \partial\hat{S}^{(n)}$ (i.e. when $\hat{f}^{(n)}(x) = 0$) so that the cSUR metric naturally enforces some exploration by sampling close to, but not exactly at, the estimated contour.

3.2 Multi-Level Batching

The most basic batching strategy is Fixed Batching (FB):

$$r_{n+1} \equiv r_0$$

for some pre-specified batching level r_0 . To improve upon FB, we select r_{n+1} from a discrete set $\mathbf{r}_L := \{r^1, \dots, r^L\}$, interpreted as representing L different *sampling fidelities*. Query at x on the

Algorithm 1 Multi-Level Batching (MLB)

Input: $\mathbf{r}_L, \eta, k_0, r_0$
 $\mathcal{A}_{k_0} \leftarrow \{(\bar{x}_i, r_0, \bar{y}_i), 1 \leq i \leq k_0\}, (\hat{f}^{(k_0)}, s^{(k_0)}) \leftarrow f|\mathcal{A}_{k_0}, \gamma \leftarrow Ave(s^{(0)}(\bar{x}_{1:k_0}))$.
 $N_{k_0} \leftarrow r_0 \times k_0$.
for $n = k_0, k_0 + 1, \dots$ **do**
 $\bar{x}_{n+1} \leftarrow \arg \max_{x \in D} \mathcal{I}_n^{MCU}(x)$.
while $s^{(n+1)}(\bar{x}_{n+1}, r^1) < \gamma$ { Check if need to lower threshold} **do**
 $\gamma \leftarrow \eta \times \gamma$.
end while
 $r_{n+1} \leftarrow \max\{r \in \mathbf{r}_L : s^{(n+1)}(\bar{x}_{n+1}, r) \geq \gamma\}$.
 $\bar{y}_{n+1} \leftarrow \frac{1}{r_{n+1}} \sum_{j=1}^{r_{n+1}} y^{(j)}$.
 Update $\mathcal{A}_{n+1} \leftarrow \mathcal{A}_n \cup \{(\bar{x}_{n+1}, r_{n+1}, \bar{y}_{n+1})\}$.
 Obtain $(\hat{f}^{(n+1)}, s^{(n+1)}) \leftarrow f|\mathcal{A}_{n+1}$.
 $N_{n+1} \leftarrow N_n + r_{n+1}$.
end for

ℓ -th level implies using r^ℓ replicates to generate observations $y^{(j)}, j = 1, \dots, r^\ell$ yielding the average \bar{y} . The cost of the ℓ -th fidelity is proportional to r^ℓ .

Kandasamy et al. [2016a] investigated multi-fidelity GP metamodels, with the idea of using low/cheap fidelities to explore and then high/expensive fidelities to exploit the desired contour. Using this strategy, we propose the MLB Algorithm 1 which first chooses the next input \bar{x}_{n+1} and then the associated number of replicates r_{n+1} . Specifically, we determine \bar{x}_{n+1} via the MCU criterion \mathcal{I}_n^{MCU} (8) and then choose r_{n+1} based on the look-ahead standard deviation $s^{(n+1)}(\bar{x}_{n+1}, \cdot)$ in (9). The choice of r_{n+1} is based on a threshold $\gamma = \gamma_n$ which acts as the target level for the next-step standard deviation. Intuitively, γ_n controls the credibility of the model; it is progressively lowered as the input space is explored. Recall that $r \mapsto s^{(n+1)}(\bar{x}_{n+1}, r)$ is monotone decreasing in (9); MLB tries to match $s^{(n+1)}(\bar{x}_{n+1}, r)$ with γ_n by choosing the *highest fidelity* $r_{n+1} \in \mathbf{r}_L$ for which $s^{(n+1)}(\bar{x}_{n+1}, r_{n+1}) > \gamma_n$. If $s^{(n+1)}(\bar{x}_{n+1}, r) > \gamma_n$ for all $r \in \mathbf{r}_L$ then we use the highest fidelity level $r_{n+1} = r^L$; if $s^{(n+1)}(\bar{x}_{n+1}, r) < \gamma_n$ for all $r \in \mathbf{r}_L$ then we lower the threshold by multiplying γ_n by a reduction factor $\eta < 1$, and try to identify r_{n+1} again, cf. Kandasamy et al. [2016a]. Note that unlike other acquisition functions, including cSUR, MCU is based solely on information in \mathcal{A}_n and hence allows to decouple the selection of \bar{x}_{n+1} from that of r_{n+1} .

3.3 Ratchet Batching

By construction, the MLB Algorithm 1 will step back and forth between different replication levels r^ℓ . Since intuitively the design should concentrate as n grows, we expect r_n to grow over time which is achieved through the decreasing γ_n . A stricter enforcement of increasing replication levels suggests a variant of MLB that restricts $n \mapsto r_n$ to be monotonically non-decreasing and reduces picking r_{n+1} among just two fidelity levels (compared to L levels in MLB). The resulting Ratchet Batching (RB) scheme is summarized in Algorithm 2. Let $r_n^\uparrow = \min\{r \in \mathbf{r}_L : r > r_n\}$ be the next level. Then RB either keeps $r_{n+1} = r_n$ if $s^{(n+1)}(\bar{x}_{n+1}, r_n) \geq \gamma_n > s^{(n+1)}(\bar{x}_{n+1}, r_n^\uparrow)$ or increments to $r_{n+1} = r_n^\uparrow$ if $s^{(n+1)}(\bar{x}_{n+1}, r_n) > s^{(n+1)}(\bar{x}_{n+1}, r_n^\uparrow) \geq \gamma_n$. In the third case where $s^{(n+1)}(\bar{x}_{n+1}, r_n) < \gamma_n$ we lower the threshold γ_n as in MLB. For RB, the reduction factor η for γ should be close to 1, to avoid excessive ratcheting up. If η is not large enough, there is a risk to skip levels in \mathbf{r}_L and to end up with excessive replication relative to number of simulation calls, leading to insufficient exploration.

Algorithm 2 Ratchet Batching (RB)

Input: $\mathbf{r}_L, \eta, k_0, r_0$
 $\mathcal{A}_{k_0} \leftarrow \{(\bar{x}_i, r_0, \bar{y}_i), 1 \leq i \leq k_0\}, (\hat{f}^{(k_0)}, s^{(k_0)}) \leftarrow f|_{\mathcal{A}_{k_0}}, \gamma \leftarrow s^{(k_0)}$.
 $N_{k_0} \leftarrow r_0 \times k_0$.
for $n = k_0, k_0 + 1, \dots$ **do**
 $\bar{x}_{n+1} \leftarrow \arg \max_{x \in D} \mathcal{I}_n^{MCU}(x)$.
while $s^{(n+1)}(\bar{x}_{n+1}, r_n) < \gamma$ {Check if need to lower threshold} **do**
 $\gamma \leftarrow \eta \times \gamma$.
end while
 $r_n^\uparrow \leftarrow \min\{r \in \mathbf{r}_L : r > r_n\}$
 $r_{n+1} \leftarrow r_n \cdot \mathbf{1}_{\{s^{(n+1)}(\bar{x}_{n+1}, r_n^\uparrow) < \gamma\}} + r_n^\uparrow \cdot \mathbf{1}_{\{s^{(n+1)}(\bar{x}_{n+1}, r_n^\uparrow) \geq \gamma\}}$
 $\bar{y}_{n+1} \leftarrow \frac{1}{r_{n+1}} \sum_{j=1}^{r_{n+1}} y^{(j)}$.
 Update $\mathcal{A}_{n+1} \leftarrow \mathcal{A}_n \cup \{(\bar{x}_{n+1}, r_{n+1}, \bar{y}_{n+1})\}$.
 Obtain $(\hat{f}^{(n+1)}, s^{(n+1)}) \leftarrow f|_{\mathcal{A}_{n+1}}$.
 $N_{n+1} \leftarrow N_n + r_{n+1}$.
end for

3.4 Adaptively Batched Stepwise Uncertainty Reduction

The FB, MLB and RB schemes all pick \bar{x}_{n+1} first and then r_{n+1} . We next propose a procedure to pick both through a joint criterion optimization. The main idea is to tie the choice of r_{n+1} to *cost*, namely to maximize the ratio of the information gain and the cost of generating r outputs, plus the optimization overhead. The inclusion of the overhead in \mathcal{I}_n comes from [Klein et al., 2017, McLeod et al., 2017], where the authors treated the total cost as the sum of query cost T_{sim} and the GP metamodeling overhead c_{ovh} . This was then extended by Swersky et al. [2013] to multi-fidelity Bayesian optimization. Stroh et al. [2017] discussed estimating a probability of exceeding a threshold in a multi-fidelity stochastic simulator, where the input \bar{x}_{n+1} and the fidelity are estimated in a sequential way. We develop an analogue for level-set estimation via a cSUR-based acquisition function

$$\mathcal{I}_n^{ABSUR}(x, r) := \frac{\mathcal{I}_n^{cSUR}(x, r)}{c(r) + c_{ovh}(n)}, \quad (11)$$

where $c_{ovh}(n)$ is the overhead and $c(r) = r \cdot T_{sim}$ is the cost of r evaluations, linear in r . Combining (11) and (9), we obtain

$$\mathcal{I}_n^{ABSUR}(x, r) := \frac{\Phi\left(-\frac{|\hat{f}^{(n)}(x)|}{s^{(n)}(x)}\right) - \Phi\left(-\frac{|\hat{f}^{(n)}(x)| \sqrt{r s^{(n)}(x)^2 + \tau^2}}{s^{(n)}(x)}\right)}{r \cdot T_{sim} + c_{ovh}(n)}. \quad (12)$$

The resulting ABSUR Algorithm 3 myopically maximizes \mathcal{I}^{ABSUR} over $x \in D$ and $r \in \mathcal{R} = [\underline{r}, \bar{r}]$. Intuitively, the location of \bar{x}_{n+1} is similar to the cSUR DoE and the value of r_{n+1} is controlled by $s^{(n)}(x)^2$ and $c_{ovh}(n)$; more replication results when $s^{(n)}(x)^2$ is small or $c_{ovh}(n)$ is large.

There are four hyperparameters in ABSUR: the simulation cost T_{sim} , the overhead cost function $c_{ovh}(n)$ and the lower/upper bounds of replication $[\underline{r}, \bar{r}]$. For $c_{ovh}(n)$ we follow the recipe in [McLeod et al., 2017], modeling it as a quadratic function of n to reflect the prediction complexity of GPs:

$$c_{ovh}(n; \boldsymbol{\theta}) = \theta_0 + \theta_1 n + \theta_2 n^2, \quad (13)$$

Algorithm 3 Adaptive Batched SUR (ABSUR)

Input: $\mathcal{R} = [r, \bar{r}]$, k_0 , r_0 , T_{sim} , overhead cost function $n \mapsto c_{ovh}(n)$
 $\mathcal{A}_{k_0} \leftarrow \{(\bar{x}_i, r_0, \bar{y}_i), 1 \leq i \leq k_0\}$, $(\hat{f}^{(k_0)}, s^{(k_0)}) \leftarrow f|_{\mathcal{A}_{k_0}}$
 $N_{k_0} \leftarrow r_0 \times k_0$
for $n = k_0, k_0 + 1, \dots$ **do**
 $(\bar{x}_{n+1}, r_{n+1}) \leftarrow \arg \sup_{x \in D, r \in \mathcal{L}} \mathcal{I}_n^{ABSUR}(x, r)$.
 $\bar{y}_{n+1} \leftarrow \frac{1}{r_{n+1}} \sum_{j=1}^{r_{n+1}} y^{(j)}$.
 Update $\mathcal{A}_{n+1} \leftarrow \mathcal{A}_n \cup \{(\bar{x}_{n+1}, r_{n+1}, \bar{y}_{n+1})\}$.
 Obtain $(\hat{f}^{(n+1)}, s^{(n+1)}) \leftarrow f|_{\mathcal{A}_{n+1}}$.
 $N_{n+1} \leftarrow N_n + r_{n+1}$.
end for

where θ are fitted empirically. Alternatively Klein et al. [2017] kept $c_{ovh}(n)$ as a constant. The value of T_{sim} represents the cost of obtaining each observation. If simulations are cheap, we would like to replicate more, and indeed lower T_{sim} leads to smaller designs. This feature implies that T_{sim} should be larger in higher-dimensional settings, since more unique inputs are needed to explore a larger input space.

4 Adaptive Design with Stepwise Allocation

The four strategies (FB, MLB, RB and ABSUR) discussed in Section 3 visit each input site \bar{x}_{n+1} only once. Consequently, the respective replicate count r_{n+1} is determined at step $n + 1$ and then remains the same throughout the latter steps. As an alternative, one can sequentially *allocate* new simulations across existing designs, thereby gradually growing $r_i^{(n)}$. Namely, the algorithm identifies existing “informative” inputs and augments their replicate counts, without changing the number of unique inputs k_n across the sequential design rounds n . In our context, we pair this augmentation with the option of expanding the design set itself. This choice is similar to the classical exploitation (do not change k_n) versus exploration (increase k_n). The resulting ADSA approach resembles *Stepwise Approximate Optimal Design (SAO)*, an IMSE-based sequential design strategy proposed by Chen and Zhou [2017] for mean response prediction.

At each step n of the ADSA strategy we are given a budget of $\Delta r^{(n)}$ additional simulations, and the main decision is to determine whether we should choose a new input \bar{x}_{k_n+1} that then receives all these $\Delta r^{(n)}$ replicates, or we should allocate the $\Delta r^{(n)}$ new simulator calls across the existing inputs $\bar{\mathbf{x}}_{1:k_n}$. In the latter case, we aim to minimize the global look-ahead integrated contour uncertainty $\mathcal{L}^{(n+1)}$ where the metric $\mathcal{L}^{(n)}$ is defined by

$$\mathcal{L}^{(n)} := \sum_{j=1}^M \omega_j^{(n)} \hat{f}^{(n)}(x_{j,*}) = (\boldsymbol{\omega}^{(n)})^T \mathbf{f}_*^{(n)} \simeq \int_D \Phi(-\hat{f}(x)/s^{(n)}(x)) \hat{f}^{(n)}(x) \mu(dx), \quad (14)$$

where $\mathbf{x}_* = x_{1,*}, \dots, x_{M,*}$ is a test set of size M (constructed using Latin Hypercube Sampling), $\mathbf{f}_*^{(n)} \equiv \hat{f}(\mathbf{x}_*)$ is the vector of predicted responses at \mathbf{x}_* , and $\omega_j^{(n)} \equiv \omega(x_{j,*}) \mu(x_{j,*}) = \Phi(-\hat{f}^{(n)}(x_{j,*})/s^{(n)}(x_{j,*})) \mu(x_{j,*})$ are the weights that target the level-set region of interest (compare to the targeted integrated mean square error (tIMSE) criterion proposed by Picheny et al. [2010]).

For allocation purposes, we approximate the look-ahead $\mathcal{L}^{(n+1)}$ as a linear combination of the M predictions $\hat{f}^{(n+1)}(x_{j,*})$ with *fixed* importance weights $\boldsymbol{\omega}^{(n)}$, whereby our goal is to minimize the variance of $(\boldsymbol{\omega}^{(n)})^T \mathbf{f}_*^{(n+1)}$ conditional on the extra allocations $\Delta r_i^{(n)}$ at each input \bar{x}_i . Since the

covariance matrix of $\mathbf{f}_*^{(n+1)}$ given replication counts $\mathbf{R}^{(n+1)}$ is

$$\mathbf{C}^{(n+1)} = \mathbf{k}(\mathbf{x}_*, \mathbf{x}_*) - \mathbf{k}(\mathbf{x}_*, \bar{\mathbf{x}}_{1:k_n})(\mathbf{K} + \tau^2 \mathbf{R}^{(n+1)})^{-1} \mathbf{k}(\mathbf{x}_*, \bar{\mathbf{x}}_{1:k_n})^T \quad (15)$$

the objective becomes the quadratic program

$$\mathcal{I}_{SAO}((\Delta r_i)_{i=1}^{k_n}) = (\boldsymbol{\omega}^{(n)})^T \mathbf{C}^{(n+1)} \boldsymbol{\omega}^{(n)} \mapsto \min! \quad (16)$$

under the constraint $\sum_i \Delta r_i^{(n)} = \Delta r^{(n)}$.

Define the $k_n \times k_n$ matrix $\boldsymbol{\Sigma}^{(n)} = \mathbf{K} + \tau^2 \mathbf{R}^{(n)}$ and the $M \times k_n$ matrix $\mathbf{K}_* := \mathbf{K}(\mathbf{x}_*, \bar{\mathbf{x}}_{1:k_n})$. The next proposition, proven in Section 4.1, explains how to pick $\Delta r_i^{(n)}$'s to minimize (16).

Proposition 4.1. *Let $\Delta \mathbf{R}^{(n)} := \mathbf{R}^{(n)} - \mathbf{R}^{(n+1)}$ be a $k_n \times k_n$ diagonal matrix with elements $\Delta \mathbf{R}_{ii}^{(n)} = \frac{\Delta r_i^{(n)}}{(r_i^{(n)} + \Delta r_i^{(n)})r_i^{(n)}} = [r_i^{(n)}]^{-1} - (r_i^{(n)} + \Delta r_i^{(n)})^{-1}$, $i = 1, \dots, k_n$. Assume $\max_{i=1, \dots, k_n} \Delta \mathbf{R}_{ii}^{(n)} \ll 1$. The optimal allocation rule that minimizes (16) is to assign $\Delta r_i^{(n)}$ to each \bar{x}_i such that*

$$r_i^{(n)} + \Delta r_i^{(n)} \propto \mathbf{U}_i^{(n)}, \quad (17)$$

where

$$\mathbf{U}^{(n)} = (\boldsymbol{\Sigma}^{(n)})^{-1} \mathbf{K}_*^T \boldsymbol{\omega}^{(n)}. \quad (18)$$

After obtaining the allocations $\Delta \mathbf{r}_{1, \dots, k_n}^{(n)}$, we compute the resulting look-ahead tIMSE metric:

$$\mathcal{I}_{SAO}^{(n)-all} := \sum_{j=1}^M \tilde{s}^{(n+1)}(x_{j,*})^2 \omega_j^{(n)}, \quad (19)$$

where the look-ahead variance $\tilde{s}^{(n+1)}(\cdot)^2$ is based on the new replicate counts $r_i^{(n+1)} = r_i^{(n)} + \Delta r_i^{(n)}$, $i = 1, \dots, k_n$, see proof in [Chevalier et al., 2014b, Hu and Ludkovski, 2017]:

$$\tilde{s}^{(n+1)}(\mathbf{x}_*)^2 = s^{(n)}(\mathbf{x}_*)^2 - \mathbf{k}_*(\boldsymbol{\Sigma}^{(n)})^{-1} \Delta \mathbf{R}^{(n)} (\boldsymbol{\Sigma}^{(n)})^{-1} \mathbf{k}_*^T. \quad (20)$$

The alternative to allocating over existing $\bar{\mathbf{x}}_{1:k_n}$ is to pick a new input x_{k_n+1} and assign it $\Delta r^{(n)}$ simulations. To do so, we use the MCU criterion to make it consistent with FB, MLB and RB. (Other acquisition functions can also be used and experiments suggest that the algorithm is not sensitive to this choice.) Then we evaluate the resulting $\mathcal{I}_{SAO}^{(n)-new}$:

$$\mathcal{I}_{SAO}^{(n)-new} := \sum_{j=1}^M s^{(n+1)}(x_{j,*}, \Delta r^{(n)})^2 \omega_j^{(n)}, \quad (21)$$

$$s^{(n+1)}(x_{j,*}, \Delta r^{(n)})^2 = s^{(n)}(x_{j,*})^2 - \frac{v^{(n)}(x_{j,*}, \bar{x}_{k_n+1})^2}{\frac{\tau^2}{\Delta r^{(n)}} + s^{(n)}(\bar{x}_{k_n+1})^2}.$$

The sums in (19)-(21) are used as approximations of the underlying integrals over $x \in D$. Finally, we compare $\mathcal{I}_{SAO}^{(n)-new}$ and $\mathcal{I}_{SAO}^{(n)-all}$ to determine whether to sample at the new \bar{x}_{k_n+1} or to allocate to existing $\mathbf{x}_{1:k_n}$, picking the maximum of the two tIMSE metrics.

For FB, MLB, RB and ABSUR, as we select one new input at each step, we have $k_n = n$. However, for ADSA we either select a new input or re-allocate, so that the resulting design size

Algorithm 4 Adaptive Design with Stepwise Allocation (ADSA)

Input: $\bar{\mathbf{x}}_*$, $\bar{\mathbf{x}}_{1:k_0}$, k_0 , r_0 , c_{bt}

$\mathcal{A}_{k_0} \leftarrow \{(\bar{x}_i, r_0, \bar{y}_i), i = 1, \dots, k_0\}$. $(\hat{f}^{(k_0)}, s^{(k_0)}) \leftarrow f|\mathcal{A}_{k_0}$, $N_0 \leftarrow r_0 \times k_0$.

for $n = k_0, k_0 + 1, \dots$ **do**

$\Delta r^{(n)} \leftarrow c_{bt} \sqrt{n}$.

Calculate allocations $\Delta r_i^{(n)}$, $1 \leq i \leq k_n$ with Algorithm 5.

$\bar{x}_{k_n+1} \leftarrow \arg \max_{x \in D} \mathcal{I}_n^{MCU}(x, \Delta r^{(n)})$.

Calculate $\mathcal{I}_{SAO}^{(n)-all}$, $\mathcal{I}_{SAO}^{(n)-new}$ in (21) and (19).

Case 1:

New $\bar{y}_{k_n+1} \leftarrow \frac{1}{\Delta r^{(n)}} \sum_{j=1}^{\Delta r^{(n)}} y^j(\bar{x}_{k_n+1})$.

Update $\mathcal{A}_{n+1} \leftarrow \mathcal{A}_n \cup \{(\bar{x}_{k_n+1}, \Delta r^{(n)}, \bar{y}_{k_n+1})\}$.

$N_{n+1} \leftarrow N_n + \sum_i \Delta r_i^{(n)}$ (May not be exactly $\Delta r^{(n)}$).

$k_{n+1} \leftarrow k_n + 1$.

Case 2:

For $i = 1, \dots, k_n$, update $\bar{y}_i \leftarrow \frac{\bar{y}_i \times r_i^{(n)} + \sum_{j=1}^{\Delta r_i^{(n)}} y^j(\bar{x}_i)}{r_i^{(n)} + \Delta r_i^{(n)}}$, $r_i^{(n+1)} \leftarrow r_i^{(n)} + \Delta r_i^{(n)}$

Update $\mathcal{A}_{n+1} \leftarrow \{(\bar{x}_i, r_i^{(n+1)}, \bar{y}_i)\}_{i=1, \dots, k_n}$.

$N_{n+1} \leftarrow N_n + \sum_{i=1}^{k_n} \Delta r_i^{(n)}$

$k_{n+1} \leftarrow k_n$

Obtain $(\hat{f}^{(n+1)}, s^{(n+1)}) \leftarrow f|\mathcal{A}_{n+1}$.

ADSA: **Do Case 1** if $\mathcal{I}_{SAO}^{(n)-all} > \mathcal{I}_{SAO}^{(n)-new}$, **otherwise do Case 2**

{FDSA variant:} **Do Case 2.**

{DDSA variant:} **Do Case 1** if n is odd, **Case 2** if n is even.

end for

satisfies $k_n < n$. Thus, relative to the earlier schemes, in ADSA the size of \mathcal{A}_n and the number of DoE rounds n are no longer deterministically linked and the number of unique inputs is endogenous to the particular algorithm run.

A major goal of all our schemes is for k_n to grow sub-linearly in n , i.e. new inputs are added less frequently as more simulations are run. In ADSA, this translates into endogenously preferring re-allocation over adding inputs as n . The user can further preference this situation by making the batches $\Delta r^{(n)}$ also grow in n . Specifically, we have found a good heuristic in taking $\Delta r^{(n)}$ to be proportional to \sqrt{n} (see proportionality constant c_{bt} in Algorithm 4), which is faster compared to constant batch sizes and more accurate than making $\Delta r^{(n)}$ linear in n which is overly aggressive.

Deterministic and Fixed DSA. In practice we observe that the ADSA scheme tends to alternate roughly equally between re-allocation and addition of new inputs. To save computational overhead, we consider the simplified *Deterministic Design with Stepwise Allocation* (DDSA) scheme that deterministically alternates between re-allocation and adding inputs, making $k_n = k_0 + \lceil (n - k_0)/2 \rceil$ also deterministic. Observe that DDSA no longer needs to evaluate the expensive $\mathcal{I}_{SAO}^{(n)-all}$ and $\mathcal{I}_{SAO}^{(n)-new}$. A different shortcut is *Fixed Design Stepwise Allocation* (FDSA) which avoids exploration altogether and keeps $k_n = K$ constant by starting immediately with a large initial design $|\mathcal{A}_0| = K$. FDSA thus always uses re-allocation, aiming to grow the number of replicates for inputs in the neighborhood of the contour. We find that the performance of FDSA is quite sensitive to the choice of the initial inputs, and k_0 needs to increase exponentially with dimension d .

4.1 Allocation Rule

Proof of Proposition 4.1. Because the unique inputs are unchanged during the allocation step, comparing $\mathbf{C}^{(n+1)} = \mathbf{K}(\mathbf{x}_*, \mathbf{x}_*) - \mathbf{K}_*(\boldsymbol{\Sigma}^{(n+1)})^{-1}\mathbf{K}_*^T$ to $\mathbf{C}^{(n)} = \mathbf{K}(\mathbf{x}_*, \mathbf{x}_*) - \mathbf{K}_*(\boldsymbol{\Sigma}^{(n)})^{-1}\mathbf{K}_*^T$, the only term that changes is $\boldsymbol{\Sigma}^{(n+1)}$.

Minimizing eq. (16) therefore reduces to maximizing

$$(\boldsymbol{\omega}^{(n)})^T \mathbf{K}_* (\mathbf{K} + \tau^2 \mathbf{R}^{(n+1)})^{-1} \mathbf{K}_*^T \boldsymbol{\omega}^{(n)} \mapsto \max! \quad (22)$$

Decompose $\Delta \mathbf{R}^{(n)} =: \mathbf{B}^{(n)} \mathbf{B}^{(n)}$. Using the Woodbury Identity,

$$(\boldsymbol{\Sigma}^{(n+1)})^{-1} = (\mathbf{K} + \tau^2 (\mathbf{R}^{(n)} - \Delta \mathbf{R}^{(n)}))^{-1} \approx (\boldsymbol{\Sigma}^{(n)})^{-1} + \tau^2 (\boldsymbol{\Sigma}^{(n)})^{-1} \Delta \mathbf{R}^{(n)} (\boldsymbol{\Sigma}^{(n)})^{-1}, \quad (23)$$

where the last expression is obtained by dropping the term $\mathbf{B}^{(n)} [\mathbf{K} + \tau^2 \mathbf{R}^{(n)}]^{-1} \mathbf{B}^{(n)} \approx \mathbf{0}$ due to $\max_i \Delta \mathbf{R}_{ii}^{(n)} \ll 1$. Therefore, maximizing (22) subject to $\sum_{i=1}^{k_n} \Delta r_i^{(n)} = \Delta r^{(n)}$ is equivalent to maximizing

$$\tilde{\mathcal{L}}_{SAO}(\Delta \mathbf{R}) = \tau^2 \cdot (\boldsymbol{\omega}^{(n)})^T \mathbf{K}_* (\boldsymbol{\Sigma}^{(n)})^{-1} \Delta \mathbf{R}^{(n)} (\boldsymbol{\Sigma}^{(n)})^{-1} \mathbf{K}_*^T \boldsymbol{\omega}^{(n)} + \lambda \left(\Delta r^{(n)} - \sum_{i=1}^{k_n} \Delta r_i^{(n)} \right), \quad (24)$$

where λ is a Lagrange multiplier. The first-order optimality conditions are

$$\frac{\partial \tilde{\mathcal{L}}_{SAO}}{\partial \Delta r_i^{(n)}} = - \frac{\tau^2 \cdot (\boldsymbol{\omega}^{(n)})^T \mathbf{K}_* (\boldsymbol{\Sigma}^{(n)})^{-1} (\boldsymbol{\Sigma}^{(n)})^{-1} \mathbf{K}_*^T \boldsymbol{\omega}^{(n)}}{(r_i^{(n)} + \Delta r_i^{(n)})^2} - \lambda = 0 \quad (25)$$

which leads to $r_i^{(n)} + \Delta r_i^{(n)} \propto [(\boldsymbol{\Sigma}^{(n)})^{-1} \mathbf{K}_*^T \boldsymbol{\omega}^{(n)}]_i$, $1 \leq i \leq k_n$ as in (18). \square

Following Liu and Staum [2010], we use a pegging procedure [Bretthauer et al., 1999] to obtain integer-valued $\Delta r_i^{(n)}$, see Algorithm 5 in the Appendix. Note that due to the rounding, the added number of replicates $\sum_{i=1}^{k_n} \Delta r_i^{(n)}$ is not exactly $\Delta r^{(n)}$. Moreover, there are several approximations in Proposition 4.1 that render $\Delta r_i^{(n)}$ and (17) suboptimal: (1) we assume that $\max_{i=1, \dots, k_n} \Delta \mathbf{R}_{ii}^{(n)} \ll 1$; (2) we freeze the weights in (16) rather than using $\boldsymbol{\omega}^{(n+1)}$; (3) we round off to integer $\Delta r_i^{(n)}$.

Remark. Similar results about minimizing the look-ahead GP variance of a linear combination $\boldsymbol{\omega}^T \mathbf{f}$ appear in [Ankenman et al., 2010, Chen and Zhou, 2017, Liu and Staum, 2010, Ludkovski and Risk, 2018]. Relative to Ankenman et al. [2010] and Chen and Zhou [2017], we get rid of all integrals, making (17) computationally efficient. The algorithm proposed by Ludkovski and Risk [2018] relied on in-sample test set $\mathbf{x}_* = \bar{\mathbf{x}}_{1:k_n}$ while our test set is different from the existing inputs.

Last but not least, we note that Proposition 4.1 can be extended to the heteroskedastic setting by replacing the constant value τ^2 in equations (22), (23), (24) and (25) by a diagonal matrix \mathbf{S} where $\mathbf{S}_{ii} = \tau^2(x_i)$, $1 \leq i \leq k_n$. Solving eq. 25 leads to $r_i^{(n)} + \Delta r_i^{(n)} \propto \tau^2(x_i) \mathbf{U}_i^{(n)}$, $1 \leq i \leq k_n$.

5 Results

5.1 Synthetic Experiments and Computational Implementation Details

In this section we benchmark the schemes on three synthetic case studies, employing *Branin-Hoo* ($d = 2$) and *Hartman* ($d = 6$) functions. We make linear transformations to the standard setups in order to rescale the output to $[-1, 1]$ and have the zero-contour “in the middle” of the input

Table 1: Parameters for the 2-D *Branin-Hoo* and the 6-D *Hartman* experiments.

	PARAMETER	2-D <i>Branin-Hoo</i>	6-D <i>Hartman</i>
Simulation budget	N_T	2000	6000
Initial design size	k_0	20	60
Initial replicates	r_0	10	10
ADSA test set in (14)	M	500	1000
Replication levels	\mathbf{r}_L	[5, 10, 15, 20, 30, 40, 50, 60, 80,	100, 140, 180, 240, 300]
ABSUR replication range	\mathcal{R}	[5, 200]	[5, 300]
ABSUR simulation cost	T_{sim}	0.01	0.05
ABSUR overhead cost in (13)	$c_{ovh}(n)$	$\boldsymbol{\theta} = [0.137, 8.15 \times 10^{-4}, 1.99 \times 10^{-6}]$	
ADSA batch factor	c_{bt}	10	3.33

space. For the Branin-Hoo case, we further restrict and rescale the original domain to make f monotone along x^1 and to generate a single zero-contour curve. Full specifications are provided in the Online Supplement, see also Lyu et al. [2018]. The 2-D case studies with the Branin-Hoo responses employ two noise settings: (i) Gaussian $\epsilon \sim \mathcal{N}(0, 1)$; and (ii) heteroskedastic Student- t where the distribution of ϵ is input-dependent: $\epsilon(x) \sim t_{6-4x^1}(0, (0.4(4x^1 + 1))^2)$. The latter setting is to test the influence of noise mis-specification. The third case study is in 6-D using the Hartman response and noise $\epsilon \sim \mathcal{N}(0, 1)$.

The squared-exponential kernel

$$K_{se}(x, x') := \sigma_{se}^2 \exp\left(-\sum_{i=1}^d \frac{(x^i - x'^i)^2}{2\ell_i^2}\right)$$

is used throughout as the GP covariance function. The covariance hyperparameters $\boldsymbol{\vartheta} = \{\ell, \sigma_{se}^2\}$ are estimated via MLE using the `fmincon` optimizer in `MATLAB`. We re-fit $\boldsymbol{\vartheta}$ every five DoE steps and otherwise treat it as fixed across n . The noise variance is taken to be known (i.e. $\tau = 1$) in the first and third case studies. It is fitted (as an unknown constant) along with $\boldsymbol{\vartheta}$ for the experiments with Student- t simulation noise.

We use FB with $r \equiv 10$ as a baseline, and compare the performance of MLB, RB, ABSUR, ADSA and DDSA. Performance is based on the error rate \mathcal{ER} in (3), i.e. evaluating (numerically, using a testing set of size M) the symmetric difference between the true and estimated level set. This is done at a fixed simulation budget N_T , i.e. each scheme is run until N_{k_n} reaches that budget. Note that the resulting number of DoE rounds will vary scheme-by-scheme and is denoted as k_T . Recall that N_n, k_n are indexed by the DoE sequential iterations, while N_T, k_T are indexed by total budget consumed. Table 1 provides further details about the parameters specific to each scheme. To optimize the various \mathcal{I} acquisition functions we use a global, gradient-free, genetic optimization approach as implemented in the `ga` function in `MATLAB`, with tolerance of 10^{-3} and 200 generations.

Whenever we use MCU we follow the recipe in Lyu et al. [2018] and set $\rho^{(n)} = IQR(\hat{f}^{(n)})/3Ave(s^{(n)})$ which keeps both terms in (7) approximately comparable as n changes. For MLB, we initialize γ as the average standard deviation $Ave(s^{(k_0)}(\bar{x}_{1:k_0}))$ and take the reduction factor $\eta = 0.5$. For RB we use the same initial γ but decrement it slower, $\eta = 0.8$. For ABSUR, we recommend minimal replication \underline{r} of 5 or 10, and maximum replication of $\bar{r} = 0.05N_T$, i.e. 5% of the total budget N_T . The coefficients $\boldsymbol{\theta}$ in the quadratic overhead function $c_{ovh}(n)$ in (13) are pre-tuned via a linear least squares regression with the given simulator and hardware setup. For the batch factor in ADSA we take $c_{bt} = 20/d$, which favors exploration in higher-dimensional problems with larger input space.

We fit all the Gaussian Process surrogates using the `GPstuff` suite in `MATLAB` [Vanhatalo et al., 2013] although the adaptive batching heuristics are actually implemented in both `MATLAB` and `R`. For reproducibility, our supplementary material contains `R` code to reproduce Figure 6 below. We are happy to provide the Matlab codes upon request as well.

5.2 GP with Student t -Noise

Our adaptive batching strategies are not limited to the vanilla GP setup. Other metamodels can be straightforwardly substituted as long as they allow to efficiently evaluate the \mathcal{I}_n criteria and the batch look-ahead variance $s^{(n+1)}(x, r)$. As one instructive example we consider a GP approach with Student- t observation noise (henceforth t -GP). Lyu et al. [2018] showed that t -GP is a good choice in the face of noise misspecification as commonly happens for practical stochastic simulators, cf. Section 6. In the t -GP metamodel formulation ϵ_i in (2) is taken to be t -distributed with variance τ^2 and $\nu > 2$ degrees of freedom (the latter is treated as another hyperparameter) leading to the marginal likelihood of $\bar{\mathbf{y}}_{1:k_n}$ as (with $\mathbf{f} := f_{1:k_n} = (f(\mathbf{x}_1), \dots, f(\mathbf{x}_{k_n}))$)

$$p_{t\text{GP}}(\bar{\mathbf{y}}_{1:k_n} | \bar{\mathbf{x}}_{1:k_n}, \mathbf{r}_{1:k_n}^{(n)}, \mathbf{f}) = \prod_{i=1}^{k_n} \frac{\Gamma((\nu+1)/2) \sqrt{r_i^{(n)}}}{\Gamma(\nu/2) \sqrt{\nu\pi}\tau} \left(1 + \frac{r_i^{(n)}(y_i - f_i)^2}{\nu\tau^2} \right)^{-(\nu+1)/2}, \quad (26)$$

where $\Gamma(\cdot)$ is the incomplete Gamma function. To integrate (26) against the Gaussian prior $p(f|\boldsymbol{\theta})$ we use Laplace approximation [Williams and Barber, 1998]. Specifically, we use a second-order Taylor expansion of the log-likelihood around its mode, $\hat{\mathbf{f}}_{t\text{GP}}^{(n)} := \arg \max_{\mathbf{f}} p_{t\text{GP}}(\mathbf{f} | \bar{\mathbf{x}}_{1:k_n}, \bar{\mathbf{y}}_{1:k_n})$, to obtain a Gaussian approximation to the posterior $f(x_*) | \mathcal{A}_n \sim \mathcal{N}(\hat{f}_{t\text{GP}}^{(n)}(x_*), s_{t\text{GP}}^{(n)}(x_*)^2)$ with

$$\hat{f}_{t\text{GP}}^{(n)}(x_*) = \mathbf{k}(x_*) \mathbf{K}^{-1} \tilde{\mathbf{f}}_{t\text{GP}}^{(n)}, \quad (27)$$

$$\begin{aligned} v_{t\text{GP}}^{(n)}(x_*, x'_*) &= K(x_*, x'_*) - \mathbf{k}(x_*) \left(\mathbf{K} + (\mathbf{W}_{t\text{GP}}^{(n)})^{-1} \right)^{-1} \mathbf{k}(x'_*), \\ &= K(x_*, x'_*) - \mathbf{k}(x_*) (\boldsymbol{\Sigma}_{t\text{GP}}^{(n)})^{-1} \mathbf{k}(x'_*) \end{aligned} \quad (28)$$

where $\mathbf{W}_{t\text{GP}}^{(n)}$ is diagonal with

$$W_{t\text{GP},ii}^{(n)} = -\nabla^2 \log p_{t\text{GP}}(\bar{y}_i | \tilde{f}_i^{(n)}, \bar{x}_i) = (\nu+1) \frac{\nu \frac{\tau^2}{r_i^{(n)}} - (\bar{y}_i - \tilde{f}_i^{(n)})^2}{\left(\nu \frac{\tau^2}{r_i^{(n)}} + (\bar{y}_i - \tilde{f}_i^{(n)})^2 \right)^2}, \quad (29)$$

since the likelihood factorizes over observations.

Lyu et al. [2018] then calculated the approximate step-ahead variance of t -GP:

$$s_{t\text{GP}}^{(n+1)}(x_{k_n+1}, r_{k_n+1}^{(n)})^2 \simeq s_{t\text{GP}}^{(n)}(x_{k_n+1})^2 \cdot \frac{\frac{\tau^2}{r_{k_n+1}^{(n)}} \frac{\nu+1}{\nu-1}}{\frac{\tau^2}{r_{k_n+1}^{(n)}} \frac{\nu+1}{\nu-1} + s_{t\text{GP}}^{(n)}(x_{k_n+1})^2}. \quad (30)$$

We replace Eq. (9) with (30) to obtain \mathcal{I} acquisition functions for t -GP. See Appendix B for allocation rule of t -GP.

Table 2: Scheme performance across the three synthetic case studies. Results are means (\pm standard deviations) from 50 runs of each combination of a metamodel and batching scheme.

DESIGN	MODEL	ERROR RATE \mathcal{ER}_T	TIME/S	AVE k_T
<i>2-D Branin-Hoo</i> WITH $\epsilon \sim \mathcal{N}(0, 1)$				
FB	GP	0.019 \pm 0.005	118.89	200.00
ABSUR	GP	0.021 \pm 0.007	10.32	35.20
RB	GP	0.021 \pm 0.008	8.30	38.72
MLB	GP	0.018 \pm 0.008	8.63	38.44
ADSA	GP	0.020 \pm 0.008	14.11	34.42
DDSA	GP	0.022 \pm 0.007	7.92	37.00
<i>2-D Branin-Hoo</i> WITH $\epsilon \sim t_{6-4x^1}(0, (0.4(4x^1 + 1))^2)$				
FB	GP	0.034 \pm 0.029	106.37	200.00
ABSUR	GP	0.037 \pm 0.039	15.50	39.14
RB	GP	0.039 \pm 0.035	10.93	39.92
MLB	GP	0.041 \pm 0.041	11.61	42.26
ADSA	GP	0.033 \pm 0.042	18.20	34.82
DDSA	GP	0.034 \pm 0.043	9.67	37.00
FB	<i>t</i> -GP	0.024 \pm 0.010	192.44	200.00
ABSUR	<i>t</i> -GP	0.036 \pm 0.014	29.55	35.00
RB	<i>t</i> -GP	0.032 \pm 0.014	23.65	39.66
MLB	<i>t</i> -GP	0.030 \pm 0.018	22.88	39.72
ADSA	<i>t</i> -GP	0.031 \pm 0.013	26.26	30.68
DDSA	<i>t</i> -GP	0.034 \pm 0.018	15.30	37.00
<i>6D Hartman</i> WITH $\epsilon \sim \mathcal{N}(0, 1)$ AND $N_T = 6000$				
FB	GP	0.030 \pm 0.004	1934.51	600.00
ABSUR	GP	0.070 \pm 0.015	289.52	159.80
RB	GP	0.058 \pm 0.014	104.68	143.40
MLB	GP	0.037 \pm 0.008	294.49	240.62
ADSA	GP	0.043 \pm 0.007	198.82	171.74
DDSA	GP	0.050 \pm 0.009	101.59	142.00
<i>6D Hartman</i> WITH $\epsilon \sim \mathcal{N}(0, 1)$ AND $N_T = 30000$				
FB $r_n = 50$	GP	0.015 \pm 0.002	1654.32	600.00
FB $r_n = 100$	GP	0.016 \pm 0.002	461.57	330.00
FB $r_n = 200$	GP	0.029 \pm 0.006	152.21	195.00
ABSUR	GP	0.022 \pm 0.003	757.18	325.25
RB	GP	0.024 \pm 0.005	227.01	237.05
MLB	GP	0.022 \pm 0.006	240.61	242.95
ADSA	GP	0.016 \pm 0.002	995.57	373.80
DDSA	GP	0.017 \pm 0.002	522.00	350.00

5.3 Algorithm Performance

Our main goal with adaptive batching is improved computational performance. Of course, a faster algorithm generally requires to sacrifice predictive accuracy. As such, direct comparison of schemes is not possible but must be considered through the above trade-off. Figure 1 and Table 2 show the link between the error rate \mathcal{ER} from (3) and the running time across the proposed scheme. Since we desire fast and accurate schemes, there is a Pareto frontier going from top-left to bottom-right. In the 2-D case study (shown in the left panel in Figure 1), we see that the most accurate scheme is *t*-GP with FB, while the fastest is GP with DDSA. Another Pareto-efficient scheme is *t*-GP with MLB which is arguably the best (the second fastest among *t*-GPs, and the second most accurate). In 6-D ABSUR works poorly, probably due to under-performance of the cSUR criterion; see Lyu et al. [2018] who showed that MCU appears to be empirically better for this 6-D Hartman function. Another reason is that cSUR converges in a slower rate, see the middle panel in Figure 2: cSUR

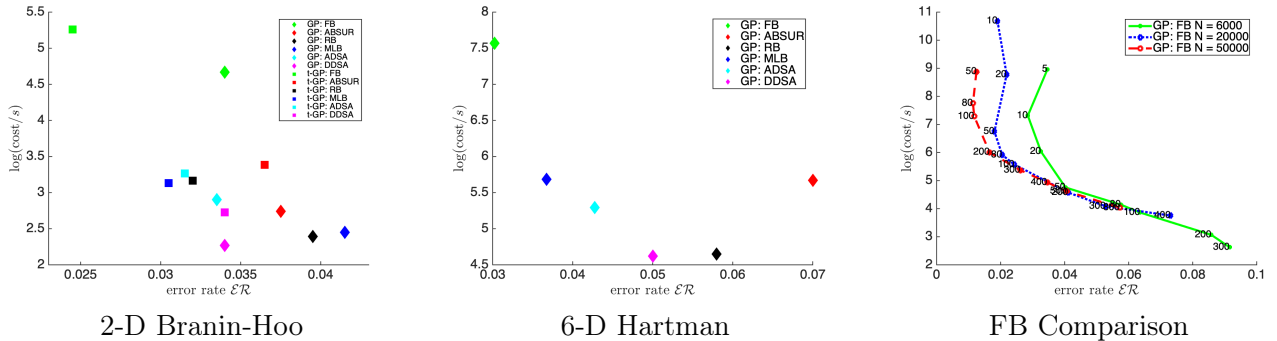


Figure 1: Running time and ultimate error rate $\mathcal{E}\mathcal{R}_T$ across different schemes. *Left panel:* 2-D Branin-Hoo with Student- t noise and budget $N_T = 2000$. *Middle panel:* 6-D Hartman function with Gaussian noise and $N_T = 6000$. *Right panel:* 6-D Hartman function with Gaussian noise for FB with different values of r .

takes $N_T \approx 30000$ simulations to achieve a comparably small error rate $\mathcal{E}\mathcal{R}$. However, in Figure 1, $N_T = 6000$ for 6-D experiments. The best choice are MLB and ADSA, as DDSA and RB gain some speed but only at significant increase in $\mathcal{E}\mathcal{R}$.

Looking at the running times, we see that there are major gains from adaptive batching; the baseline FB scheme takes almost 10 times longer to run than adaptive batching designs. Fixed batching generally performs well in terms of $\mathcal{E}\mathcal{R}$ (as it ends up being more exploratory) but practically those gains are crowded out by the huge gains in computational efficiency. Among the five proposed schemes, MLB and ADSA tend to produce lower $\mathcal{E}\mathcal{R}$ with a significant reduction in computational time, especially in 6-D experiments.

To give some intuition about how the replication level should depend on the total budget N_T , the right panel of Figure 1 shows the performance of FB as we vary r and N_T . As expected, lower r generally leads to lower error rate $\mathcal{E}\mathcal{R}$ but longer running time. This indicates the intrinsic necessity to explore the input space adequately which introduces a lower bound regarding the number of unique inputs $k_T = N_T/r$ for FB. However, for very low r (e.g. $r < 20$ for $N_T = 6000$) there is essentially no gain from additional exploration implying that one can safely agglomerate simulations into batches without sacrificing accuracy. The resulting J-shape in the Figure implies that there is an "optimal" $r^*(N)$ that minimizes $\mathcal{E}\mathcal{R}$ without needless performance degradation: $r^*(6000) \simeq 10$, $r^*(2 \cdot 10^4) \simeq 50$, $r^*(5 \cdot 10^4) \simeq 100$. This feature showcases both the strength and the weakness of fixed batching: in principle excellent performance is possible if $r \simeq r^*$ is fine-tuned; however such fine-tuning is very difficult and without it FB can be highly inefficient. The proposed adaptive batching schemes aim to automatically fine-tune r_n sequentially removing this limitation.

Another goal of adaptive batching is to enable an organic way to grow designs as N_T changes (while for FB r necessarily must be pre-chosen in terms of N_T). A good algorithm is able to efficiently improve its accuracy as N_T grows, avoiding excessive exploration or exploitation. The right panel of Figure 2 shows the log error rate $\mathcal{E}\mathcal{R}$ as a function of N_T for FB, ABSUR, RB, MLB, ADSA and DDSA for the 6-D *Hartman* experiments, respectively. For FB, we stopped at $N_T = 6000$ due to prohibitive running times for designs. We observe that all schemes perform somewhat similarly MLB reduces the error rate $\mathcal{E}\mathcal{R}$ at the fastest rate when $N_n < 600$, and otherwise, ADSA is the fastest. ADSA shines in the later stage of sequential development of DoE, since it needs enough "candidate inputs" to calculate the allocation rule. In terms of computational efficiency, we are concerned not with $\mathcal{E}\mathcal{R}$ in terms of N_T but in terms of running time—i.e. how much predictive

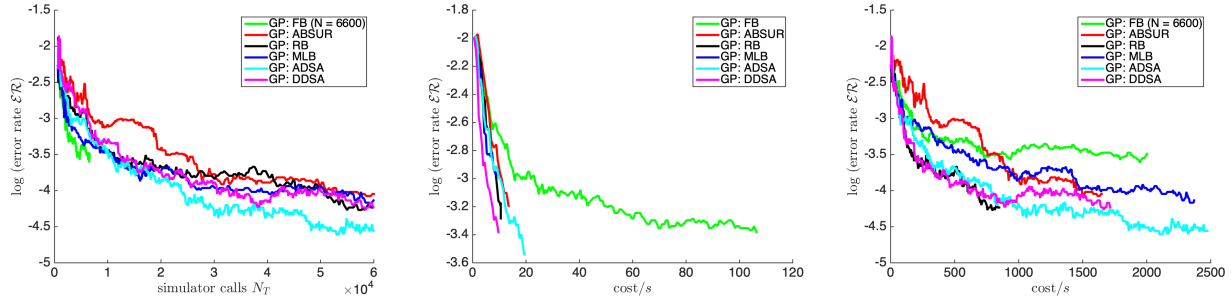


Figure 2: Log Error rate $\log \mathcal{E}\mathcal{R}_t$ as a function of simulator calls N_t for FB ($r = 10$), ABSUR, RB, MLB, ADSA and DDSA and 6-D *Hartman* experiments (left panel). Log error rate $\log \mathcal{E}\mathcal{R}_t$ as a function of running time t for 6-D *Hartman* with Gaussian noise (middle panel) with $N_T = 60000$ and for 2-D *Branin-Hoo* experiments with Student- t noise (right panel) with $N_T = 2000$. The FB algorithm is stopped at $N_t = 6000$ since computation is too slow.

accuracy can be achieved within a given time budget. The respective relationship is shown in the middle and left panels of Figure 2 where the x -axis is now in terms of t seconds. We observe that all the adaptive schemes reduce the error rate $\mathcal{E}\mathcal{R}$ at a faster rate than a scheme with fixed replication level. In the early stage, RB and DDSA are the fastest, and ABSUR is the slowest. However, as N_T continues to rise, ADSA keeps reducing the error rate $\mathcal{E}\mathcal{R}$ and eventually achieves a smaller $\mathcal{E}\mathcal{R}$ than other algorithms. However, ADSA usually takes slightly longer time. In conclusion, ADSA is the most accurate algorithm given a large enough cost t or simulator calls N_T , and MLB is the most accurate algorithm when N_T is small. Results are consistent with those observed in Figure 1.

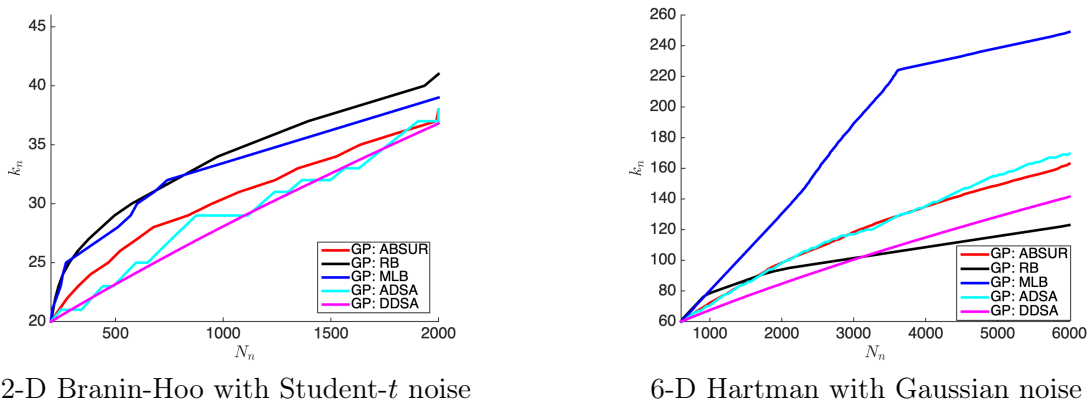


Figure 3: The design size k_n as a function of simulator calls N_n .

Recall that GP model fitting complexity is $\mathcal{O}(k_n^3)$ (driven by the matrix inversion \mathbf{K}^{-1}), so that the design size $k_n = |\mathcal{A}_n|$ is the primary driver of computational efficiency. In the baseline FB scheme, $r^{(n)} \equiv r$ is constant so that $k_n = N_n/r$ grows linearly in simulator budget N_n . This is precisely the reason that a constant r becomes impossible to maintain as N_n grows and why we had to abandon FB in the left panel of Figure 2. A key aim of adaptive batching is to achieve *sub-linear* growth of k_n i.e. $k_n/N_n \rightarrow 0$ as n grows so that $r^{(n)}$ keeps getting larger as we develop the DoE. Figure 3 plots k_n as a function of N_n for 2-D and 6-D experiments. As desired, we observe a generally concave shape, which is approximately of square-root shape. The stair-case shape of k_n for ADSA is due to the adaptive re-allocation of new simulations which allow to increase N_n

without changing k_n at some steps. We note that RB and ADSA achieve the most concave shape and hence would be the fastest for very large N_n which can be seen indirectly in Figure 2 as well.

5.4 Comparing Designs

To drill down into the designs obtained from different approaches, Figure 4 visualizes the adaptively batched designs produced for the 2-D Branin-Hoo experiment with Student- t noise. The left panel displays the resulting design size k_T with simulation budget of $N_T = 2000$. Recall that besides FB and DDSA, design sizes of all other schemes vary across algorithm runs (i.e. k_T depends on the particular realizations $y_{1:N_T}$), so that k_T is a random variable; in the plot we visualize its boxplot across 50 runs of each scheme. The smallest designs are obtained from ADSA (31-39 unique inputs). DDSA produces exactly $k_T = 37$ unique inputs. Recall that DDSA alternates between adding a new site and re-allocating to existing sites, while ADSA does the same adaptively; in this case we find that slightly more than half the time re-allocation is preferred. The design size k_n for ABSUR is slightly larger at 34-42. The value of k_T for RB varies from 37 to 45, while for MLB has the greatest number of unique inputs, ranging from 34 to 50. Given $N_T = 2000$ the above implies that the schemes average about $Ave(r^{(n)}) = 40$ -60 replicates per site. The middle panel of Figure 4 shows the replication level $r^{(n)}$ as a function of design size k_n for a typical run of schemes from Section 3.4, illustrating how replication is increased sequentially. Methods that raise $r^{(n)}$ faster end up with smaller design size k_T . ABSUR increases $r^{(n)}$ the fastest, with MLB having a similar pattern. With RB $r^{(n)}$ grows slower, implying that RB builds designs with more unique inputs.

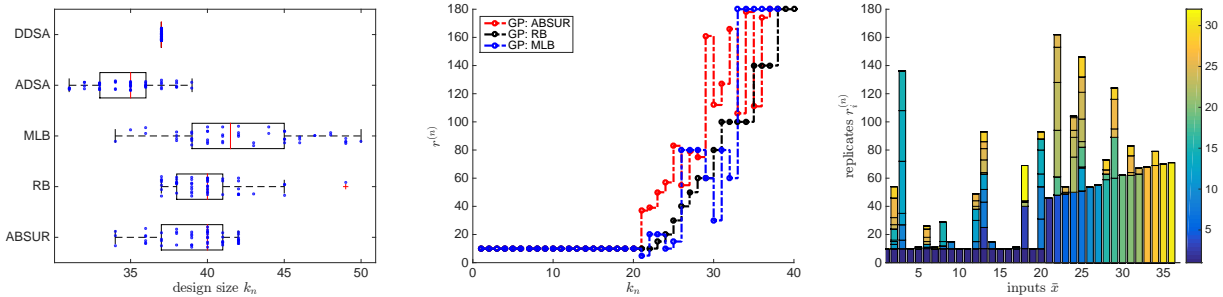


Figure 4: Visualizing adaptive batching for 2-D *Branin-Hoo* experiments with Student- t distributed noise. *Left panel*: distribution of design size k_T corresponding to $N_T = 2000$ across 50 algorithm runs. *Middle*: number of replicates $r^{(n)}$ as a function of algorithm step k_n for the schemes of Section 3. *Right*: evolution of $r_i^{(n)}$ for ADSA designs $\bar{\mathbf{x}}_{1:k_n}$. The total $r_i^{(N)}$ is decomposed into $\Delta r_i^{(n)}$ for $n = 1, \dots, k_T$ with each Δr color-coded by round n .

The right panel of Figure 4 visualizes the replication of a representative ADSA run which has the option to add new inputs or re-allocate to existing ones. We show the sequential growth of $r_i^{(n)}$ through a stack histogram: the x -axis represents the unique inputs \mathbf{x}_i as picked by the algorithm and the vertical stacks represent $\Delta r_i^{(n)}$, color-coded by the round n when they were added. We observe that only 10 out of the $n_0 = 20$ original inputs are revisited, and generally about half of the inputs are used in more than one round. At the same time, some inputs, such as $\bar{x}_{13}, \bar{x}_{20}, \bar{x}_{25}$ are visited in numerous rounds.

Figure 5 shows the estimated zero-contour $\partial \hat{S}$ with its 95% posterior credible band at $N_T = 2000$ in the 2-D test case with Gaussian noise. The volume of the credible band $\partial \hat{S}^{(\pm 0.95)}$, defined as

$$\partial \hat{S}^{(\pm 0.95)} = \left\{ x \in D : \left(\hat{f}^{(N_T)}(x) + 1.96s^{(N_T)}(x) \right) \left(\hat{f}^{(N_T)}(x) - 1.96s^{(N_T)}(x) \right) < 0 \right\}, \quad (31)$$

captures inputs x whose sign classification remains ambiguous and quantifies the uncertainty about the estimated zero-contour $\partial\hat{S}$. As expected, all schemes start by exploring the input space using a few replicates and then primarily sample in the target region around the level set, with increasing replication. Comparing the first four plots, we find that the ABSUR is more efficient than RB and MLB, concentrating at the zero-contour faster and simultaneously faster ramp-up of $r^{(n)}$. In the plot, this happens already after just half-a-dozen steps. In contrast, RB takes about a dozen steps to explore with correspondingly low $r^{(n)}$'s. Although MLB also ramps up r_n quickly, it then steps back and forth between low and high replication levels, resulting in a slightly larger k_T than ABSUR. ADSA and DDSA perform similarly. One observation is that they select similar inputs to allocate the extra simulator calls. For example the initial inputs close to the left and bottom edge all get more replicates r_n via reallocation in ADSA and DDSA. Another example is the initial input in the upper left corner of the space gets the most replicates (color yellow) compared with all other inputs for both algorithms. Across the DoE rounds, ADSA chooses to reallocate budget in approximately 54% of them, so that $k_T = 0.54N_T/\Delta r$. Therefore, the value of k_T is approximately the same for ADSA and DDSA. Some of the design differences can be attributed to the different behavior of the underlying heuristics MCU and cSUR. Indeed MCU tends to over-emphasize sampling around the zero-contour, while cSUR is more exploratory and tends to place a few inputs right at the edge of the input domain (upper left corner and lower right corner in the plot with ABSUR). The aggressiveness of MCU generates more accurate estimates $\partial\hat{S}$ even if the posterior uncertainty is higher (CI band is wider) sometimes.

To conclude, the performance of FB is sensitive to value of replicates r_n . With higher r_n , the running time decreases while the error rate \mathcal{ER} may increase or decrease. For different budget N_T , the "optimal" value of r_n varies. We can tune r_n to obtain FB scheme with best performance for a fixed N_T in synthetic experiments where the ground truth is known. However, N_T is not always provided initially in real experiments. At this time, it is impossible to tune r_n for FB. Adaptive batching designs stand out perfectly. Instead of tuning r_n manually at the start of sequential design, adaptive batching algorithms self-adaptively pick the current "optimal" r_n during sequential design. Among all adaptive batching designs, DDSA and RB are the most efficient algorithms, while ADSA ends up with the most accurate estimate in most cases with approximately twice of running time. For low dimension experiments or larger N_T , DDSA reaches similar or even better error rate \mathcal{ER} compared with ADSA, while in high dimension experiments or smaller N_T , results obtained with ADSA are significantly better than DDSA.

6 Application to Optimal Stopping

As a fourth and final case study, we consider an application of contour finding for determining the optimal exercise policy of a Bermudan financial derivative [Ludkovski, 2018]. The underlying simulator is based on a d -dimensional geometric Brownian motion $(\mathbf{Z}_t) = (z_t^1, \dots, z_t^d)$ that represents prices of d assets and follows the log-normal dynamics

$$\mathbf{Z}_{t+\Delta t} = \mathbf{Z}_t \exp \left(\left(r - \frac{1}{2} \text{diag} \mathbf{\Xi} \right) \Delta t + \sqrt{\Delta t} \mathbf{\Xi} \Delta \mathbf{W}_t \right), \quad (32)$$

where r is the interest rate, $\mathbf{\Xi}$ is the $d \times d$ covariance matrix and $\Delta \mathbf{W}_t \sim \mathcal{N}(0, \mathbf{I}_d)$ are the Gaussian stochastic stocks. Let $h(t, z)$ be the option payoff from exercising when $\mathbf{Z}_t = z$. We assume that exercising is allowed every Δt time units, up to the option maturity T . The overall goal is to determine the stopping regions $\{S_t : t = \Delta t, 2\Delta t, \dots, T - \Delta t\}$ to maximize $\mathbb{E}[h(\tau, \mathbf{Z}_\tau)]$, where $\tau = \min\{t : \mathbf{Z}_t \in S_t\}$ is the exercise strategy. The dynamic programming principle implies that S_t can be

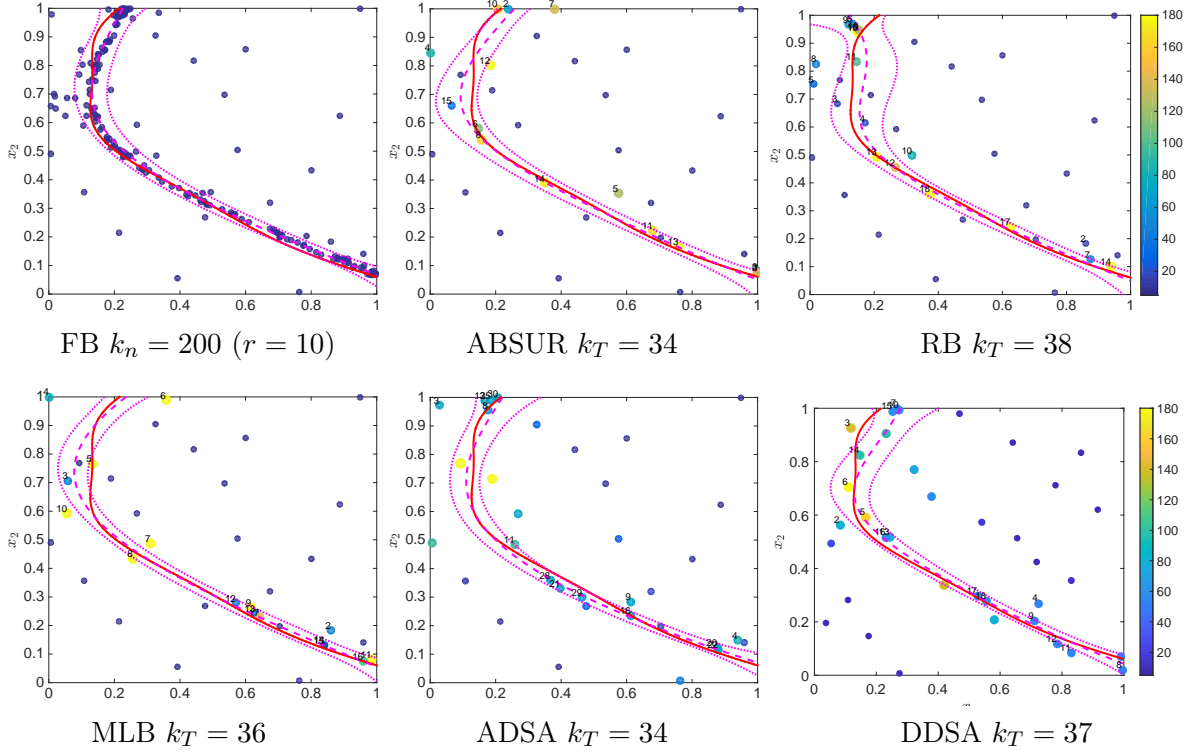


Figure 5: GP fits $f|\mathcal{A}_{k_T}$ and designs for 2-D Branin-Hoo case study with Gaussian noise. The dashed lines are the estimated posterior zero-contours $\hat{f}^{(N)}(x) = 0$ to be compared to the true contour (solid line). The dotted lines are the corresponding 95% credible intervals. The labels indicate the order of the inputs $\bar{x}_i, i = 1, \dots, k_n$ and the respective color/size are proportional to replication level $r^{(n)}$. Design sizes k_T vary across the schemes.

recursively computed as the zero level set of the timing function $z \mapsto f(t, z) = h(t, z) - \mathbb{E}[h(\tau_t, \mathbf{Z}_{\tau_t})]$ where the latter term is the continuation value based on the exercise strategy from the forward-looking $\{S_s, s > t\}$. Numerically, this yields a simulator of $f(t, z)$ through pathwise reward over one-step-ahead simulations of $\mathbf{Z}_{t+\Delta t}$.

In this setting, the underlying distribution of \mathbf{Z}_t at time t is log-normal since $\log \mathbf{Z}_t$ is multivariate normal. To reflect this fact which dictates the importance of correctly identifying whether $x \in S_t$ or not (since option exercising decisions are made *along* trajectories of \mathbf{Z} , conditional on the given initial value $\mathbf{Z}_0 = z_0$), we employ log-normal weights $\mu(dz) = p_{\mathbf{Z}_t}(\cdot|z_0)$ in (3). We further use μ to weigh the respective \mathcal{I}_n criteria when optimizing for new inputs. In line with the problem context, we assess performance using the ultimate estimated option value. The latter is evaluated via an out-of-sample Monte Carlo simulation that averages realized payoffs along a database of $M' = 10^5$ forward paths $z_{0:T}^{1:M'}$:

$$\hat{V}(0, z_0) = \frac{1}{M'} \sum_{m=1}^{M'} h(\tau_0^m, z_{\tau_0^m}^{(m)}), \quad (33)$$

with $\tau_0^m := \min\{t : z_t^{(m)} \in \hat{S}_t\} \wedge T$. Since our goal is to find the *best* exercise value, higher \hat{V} 's indicate a better approximation of $\{S_t\}$. To allow a direct comparison, we set parameters matching

Table 3: Performance of GP metamodels with FB, MLB, RB, ABSUR, ADSA and DDSA designs in the 2-D Average Put and 3-D Max Call examples. Results are averages from 20 runs of each scheme.

DESIGN	MODEL	PAYOFF	TIME/s T	INPUTS k_T
2-D AVERAGE PUT				
FB	GP	1.451± 0.002	29.82	100.00
RB	GP	1.443± 0.004	5.42	35.85
MLB	GP	1.440± 0.004	4.92	33.97
ABSOR	GP	1.446± 0.004	11.40	53.80
ADSA	GP	1.445 ± 0.003	11.76	32.87
DDSA	GP	1.445 ± 0.003	5.42	34.00
FB	t -GP	1.449 ± 0.002	63.11	100.00
RB	t -GP	1.445 ± 0.004	11.36	36.39
MLB	t -GP	1.443 ± 0.004	10.52	35.35
ABSOR	t -GP	1.443 ± 0.004	26.13	49.79
ADSA	t -GP	1.447 ± 0.003	19.00	44.83
DDSA	t -GP	1.446 ± 0.003	11.31	34.00
3-D MAX CALL				
FB	GP	11.26 ± 0.01	2239.10	1000.00
RB	GP	11.23 ± 0.01	37.42	342.39
MLB	GP	11.24 ± 0.01	38.17	342.07
ABSOR	GP	11.23 ± 0.01	109.81	407.90
ADSA	GP	11.25 ± 0.01	194.05	460.33
DDSA	GP	11.26 ± 0.01	94.58	381.00

the test cases in Ludkovski [2018]):

$$\begin{aligned}
 \text{2-D average Put option:} & \quad h_{Put}(t, \mathbf{z}) = e^{-rt}(\mathcal{K} - z^1 - z^2)_+; \\
 \text{3-D Max-Call option:} & \quad h_{Call}(t, \mathbf{z}) = e^{-rt}(\max(z^1, z^2, z^3) - \mathcal{K})_+.
 \end{aligned}$$

These settings have very low signal-to-noise ratio, and non-Gaussian heteroskedastic noise, so $N_T \gg 10^3$ is imperative.

Table 3 shows the performance of different designs/models. In the 2-D setting the best performing scheme is DDSA. We obtain savings of 80% in computation time compared to the baseline FB scheme. For the 3-D Max Call, DDSA achieves the highest payoff, and at a fraction ($\sim 1/20$ th) of time. RB and MLB lead to slightly smaller payoff than DDSA, but with a saving of 60% in computation cost. ADSA leads to basically the same payoff as DDSA and takes approximately twice as much time compared with DDSA. ABSUR takes half the time of ADSA, leading to a lower payoff. In both 2-D and 3-D settings, ADSA and DDSA lead to a higher payoff and have a more stable performance than the other adaptive batch designs. In terms of design size k_T , ABSUR yields the largest k_T , while DDSA yields the most compact designs.

Figure 6 shows the GP fits $\hat{f}(t, \mathbf{z})$ for ABSUR and ADSA for the 2-D Put case study at $t = 0.6$. The desired zero-level contour goes from NW to SE and due to the chosen setting should be symmetric about the $z^1 = z^2$ line. We see that both strategies select inputs around the contour; consistent with the results shown in Figure 5, ABSUR is somewhat more exploratory and yields wider credible intervals for the exercise boundary $\{\hat{f}^{(k_T)} = 0\}$ in regions close to the edge of

Table 4: Parameters for the 2-D Basket Put Option and 3-D Max Call Option.

	2-D Basket Put	3-D Max-Call
Option	$\mathcal{K} = 40, \Delta t = 0.04, T = 1$	$\mathcal{K} = 100, \Delta t = 1/3, T = 3$
Parameters	$r = 0.06, \sigma = 0.2, X_0 = [40, 40]$	$r = 0.05, \sigma = 0.2, X_0 = [90, 90, 90]$
Budget	$N_T = 2000, k_0 = 20, r_0 = 20$	$N_T = 30,000, k_0 = 300, r_0 = 30$
FB	$r = 20$	$r = 30$
MLB/RB	$\mathbf{r}_L = \{20, 30, 40, 50, 60, 80, 120, 160\}$	$\mathbf{r}_L = \{20, 30, 40, 50, 80, 160, 240, 320, 480, 640\}$
ABSUR	$\mathcal{R} = [20, 160], T_{sim} = 0.01$	$\mathcal{R} = [20, 640], T_{sim} = 0.01$
ADSA	$c_{bt} = 10$	$c_{bt} = 6.67$

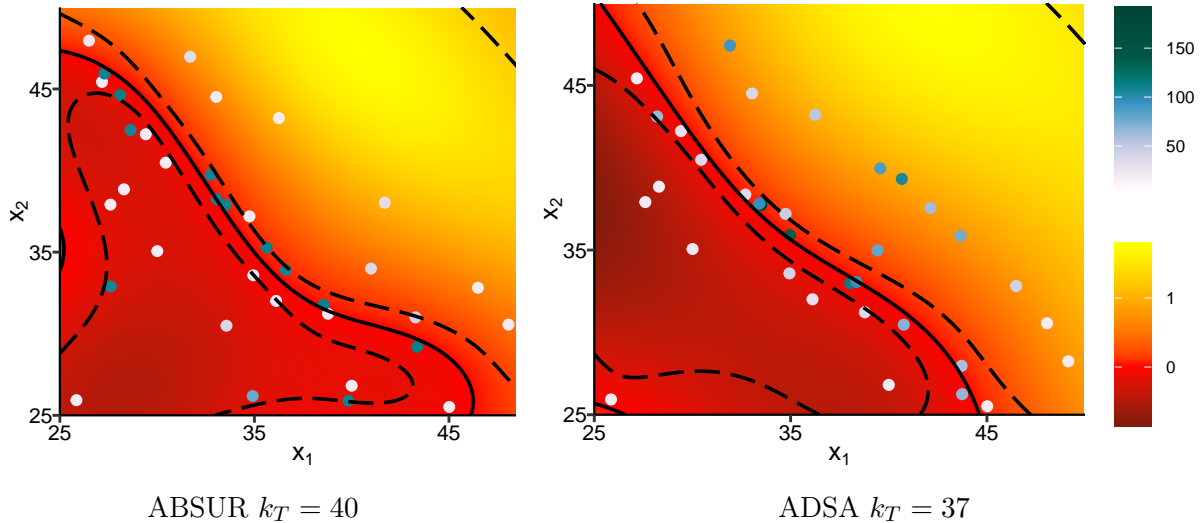


Figure 6: GP fits $f^{(k_T)}(t, \cdot)$ and designs \mathcal{A} for 2-D average put option example at $t = 0.6$ and $N_T = 2000$. *Left panel*: ABSUR; *right*: ADSA. The solid lines are the estimated exercise boundary $\hat{f}^{(k_T)}(t, \mathbf{z}) = 0$ and the dashed lines are the corresponding 95% credible intervals. The scatter plot is the design \mathcal{A}_{k_T} color-coded by replicate counts $r_i, i = 1, \dots, k_T$.

the input space, especially at the NW and SE corners. ABSUR uses slightly more design sites $k_T(\text{ABSUR}) = 40 > k_T(\text{ADSA}) = 37$ and has a flatter distribution of replication counts. In contrast, ADSA uses up to $\max_n r^{(n)} = 188$ replicates. We also observe that several initial designs repeatedly receive more replications (up to 50 counts) in ADSA.

7 Conclusion

We have proposed and investigated five different schemes for adaptive batching in metamodeling of stochastic experiments. All schemes successfully capture the intuition of increasingly beneficial replication as sequential design is constructed and the focus shifts from exploration to exploitation. Our algorithms are based on the plain Gaussian Process paradigm but are easily extended to related non-Gaussian frameworks, as demonstrated with t -GP. The key step is to construct an approximation of the batch look-ahead variance $s^{(n+1)}(x, r)$. Our results demonstrate that adaptive batching offers a simple mechanism to extract significant computational gains through building more

compact designs and taking advantage of the symbiotic relationship between GPs and replication. Thus, compared with using a constant value for replicates r over all inputs like in FB, we are able to gain more than an order-of-magnitude speed-up with minimal loss of metamodeling fidelity with adaptive batching designs for noisy level set estimation problems. Among the proposed adaptive batching schemes, we advocate the use of ADSA and DDSA (the latter being essentially a faster heuristic). While they lead to similar results in lower dimensional experiments, ADSA is shown to be more accurate in complex settings, such as higher dimensions or low signal to noise ratio.

Our focus has been on adaptive batching in the context of level-set estimation. Related problems such as evaluating the probability of failure, or evaluating a tail risk measure, would benefit from the same ideas and will be investigated in follow-up projects. Another important problem that is beyond the scope of the present work is theoretical analysis about the asymptotic complexity of the proposed schemes such as ADSA, for example to establish the long-run growth rate of k_n in order to quantify the asymptotic complexity of the GP metamodel as $N_n \rightarrow \infty$.

A Pegging Algorithm for ADSA

We employ the pegging Algorithm 5 (cf. [Bretthauer et al., 1999]) to obtain the integer-valued allocation $\Delta \mathbf{r}_{1,\dots,k_n}^{(n)}$ of new replicates at existing inputs.

Algorithm 5 Pegging Algorithm

Input: $I_0 = \{1, \dots, k_n\}$, $r = \sum_{i=1}^{k_n} r_i^{(n)}$, $\mathbf{U}^{(n)}$ from eq. (18)
 $j \leftarrow 0$.
for all $i \in I_j$ **do**
 $\Delta r_i^{(n)} \leftarrow \frac{\mathbf{U}_i^{(n)}}{\sum_{j=1}^{k_n} \mathbf{U}_j^{(n)}} \times r - r_i^{(n)}$
if $\Delta r_i^{(n)} \geq 0$ **for all** $i \in I_j$ **then**
break
else
 $I_{j+1} \leftarrow \{i \in I_j : \Delta r_i^{(n)} > 0\}$
 $\Delta r_i^{(n)} = 0$ **for** $i \notin I_{j+1}$
 $r \leftarrow r - \sum_{i \in I_j, i \notin I_{j+1}} r_i^{(n)}$
 $j \leftarrow j + 1$
end if
end for
Round all $\Delta r_i^{(n)}$, $i = 1, \dots, k_n$ to the nearest integer.
(If $\sum_{i=1}^{k_n} \Delta r_i^{(n)} = 0$, round $\max_{i=1}^{k_n} \Delta r_i^{(n)}$ up to the next integer)

B Allocation Rule for t -GP

To implement ADSA and DDSA for t -GP we need (i) the analogue of Proposition 4.1 for the allocation rule $\Delta \mathbf{r}_{1:k_n}^{(n)}$ over the existing inputs $\bar{\mathbf{x}}_{1:k_n}$; (ii) the look-ahead variance $s^{(n+1),new}(x_*)$ conditional on adding a new input; (iii) look-ahead variance $s^{(n+1),all}(x_*)$ conditional on allocating $\Delta \mathbf{r}_{1:k_n}^{(n)}$. For all these tasks, the non-Gaussian likelihood (26) underlying t -GP calls for further approximations provided in the following three Lemmas.

Lemma B.1 (Allocation Rule). The allocation $\Delta \mathbf{r}_{1:k_n}^{(n)}$ is like in Proposition 4.1 but relies on

$$\tilde{\mathbf{U}}_{t\text{GP}}^{(n)} = (\tilde{\Sigma}_{t\text{GP}}^{(n)})^{-1} \mathbf{K}_*^T \boldsymbol{\omega}^{(n)}, \quad \text{with} \quad \tilde{\Sigma}_{t\text{GP}}^{(n)} := \left(\mathbf{K} + \frac{\nu+1}{\nu-1} \tau^2 \mathbf{R}^{(n)} \right). \quad (34)$$

Proof of Lemma B.1. For t -GP, the noise matrix $\tau^2 \mathbf{R}^{(n)}$ in eq. (5) is replaced with $(\mathbf{W}_{t\text{GP}}^{(n)})^{-1}$. To calculate the ADSA/DDSA allocation rule with a t -GP metamodel we substitute $(\bar{y}_i - \tilde{f}_{t\text{GP}}^{(n)}(\bar{x}_i))^2 \cong \frac{\tau^2}{r_i^{(n)}}$ and $\tilde{f}_{t\text{GP}}^{(n)}(\bar{x}_i) \cong \tilde{f}_{t\text{GP}}^{(n+1)}(\bar{x}_i)$ in eq. (29) to obtain (cf. Lyu et al. [2018])

$$\begin{aligned} W_{ii}^{(n)} &= (\nu+1) \frac{\nu \frac{\tau^2}{r_i^{(n)}} - (\bar{y}_i - \tilde{f}_i^{(n)})^2}{\left(\nu \frac{\tau^2}{r_i^{(n)}} + (\bar{y}_i - \tilde{f}_i^{(n)})^2 \right)^2} \\ &\cong (\nu+1) \frac{\nu \frac{\tau^2}{r_i^{(n)}} - \frac{\tau^2}{r_i^{(n)}}}{\left(\frac{\tau^2}{r_i^{(n)}} + \nu \frac{\tau^2}{r_i^{(n)}} \right)^2} = \frac{(\nu-1)r_i^{(n)}}{(\nu+1)\tau^2} := \widetilde{W}_{ii}^{(n)}. \end{aligned}$$

Hence, $(\mathbf{W}_{t\text{GP}}^{(n)})^{-1} \cong (\widetilde{\mathbf{W}}_{t\text{GP}}^{(n)})^{-1} = \frac{\nu+1}{\nu-1} \tau^2 \mathbf{R}^{(n)}$ and the covariance matrix $\mathbf{C}_{t\text{GP}}^{(n)}$ of $f(\mathbf{x}_*)$ is approximated as

$$\begin{aligned} \mathbf{C}_{t\text{GP}}^{(n)} &= \mathbf{K}(\mathbf{x}_*, \mathbf{x}_*) - \mathbf{K}_* \left(\mathbf{K} + (\mathbf{W}_{t\text{GP}}^{(n)})^{-1} \right)^{-1} \mathbf{K}_*^T \\ &\simeq \mathbf{k}(\bar{\mathbf{x}}_*, \bar{\mathbf{x}}_*) - \mathbf{k}_* \left(\mathbf{K} + \frac{\nu+1}{\nu-1} \tau^2 \mathbf{R}^{(n)} \right)^{-1} \mathbf{k}_*^T \\ &\simeq \mathbf{K}(\bar{\mathbf{x}}_*, \bar{\mathbf{x}}_*) - \mathbf{K}_* (\tilde{\Sigma}_{t\text{GP}}^{(n)})^{-1} \mathbf{K}_*^T, \end{aligned} \quad (35)$$

where $\tilde{\Sigma}_{t\text{GP}}^{(n)}$ matches eq. (34). The rest of the proof proceeds exactly like for the regular GP model in Proposition 4.1, after boosting τ^2 up by a constant ratio to $(\nu+1)/(\nu-1)\tau^2$. Then we obtain $\tilde{\mathbf{U}}_{t\text{GP}}^{(n)}$ as defined in (34). \square

Next, we need to approximate the next-step $\mathbf{W}_{t\text{GP}}^{(n+1)}$. Unlike in the Gaussian case where $\Sigma^{(n+1)}$ depends only on $\mathbf{R}^{(n+1)}$, for t -GP $\mathbf{W}_{t\text{GP}}^{(n+1)}$ depends on $\bar{\mathbf{y}}_{1:k_n}$ (because it depends on $\tilde{\mathbf{f}}_{t\text{GP}}$). We therefore need an approximation $\widehat{\mathbf{W}}_{t\text{GP}}^{(n+1)}$ (the notation is to emphasize that it is different from the previous approximation $\widehat{\mathbf{W}}_{t\text{GP}}^{(n)}$ to $\mathbf{W}_{t\text{GP}}^{(n)}$).

Lemma B.2 (Look-Ahead t -GP Variance). The look-ahead variance at x_* conditional on allocating $\Delta r^{(n)}$ simulations to a new input \bar{x}_{k_n+1} is approximately given by

$$\tilde{s}_{t\text{GP}}^{(n+1), \text{new}}(x_*)^2 \cong s_{t\text{GP}}^{(n)}(x_*)^2 - \frac{v_{t\text{GP}}^{(n)}(x_*, \bar{x}_{k_n+1})^2}{\frac{(\nu+1)\tau^2}{(\nu-1)\Delta r^{(n)}} + s_{t\text{GP}}^{(n)}(\bar{x}_{k_n+1})^2}. \quad (36)$$

Finally, to obtain $\mathcal{I}_{SAO}^{(n), \text{all}}$ we define

$$\widehat{W}_{ii}^{(n+1)} := (\nu+1) \frac{\nu \frac{\tau^2}{r_i^{(n+1)}} - (\bar{y}_i^{(n)} - \tilde{f}_{t\text{GP}}^{(n)}(\bar{x}_i))^2}{\left((\bar{y}_i^{(n)} - \tilde{f}_{t\text{GP}}^{(n)}(\bar{x}_i))^2 + \nu \frac{\tau^2}{r_i^{(n+1)}} \right)^2}, \quad (37)$$

based on the approximation $(\bar{y}_i^{(n+1)} - \tilde{f}_{t\text{GP}}^{(n+1)}(x_i))^2 \cong (\bar{y}_i^{(n)} - \tilde{f}_{t\text{GP}}^{(n)}(x_i))^2$. This yields

Lemma B.3 (Look-ahead t -GP variance after batch allocation).

$$\tilde{s}_{t\text{GP}}^{(n+1),\text{all}}(x_*) \cong K(x_*, x_*) - \mathbf{K}_* \left(\mathbf{K} + (\widehat{\mathbf{W}}_{t\text{GP}}^{(n+1)})^{-1} \right)^{-1} \mathbf{K}_*^T. \quad (38)$$

References

- B. Ankenman, B. L. Nelson, and J. Staum. Stochastic kriging for simulation metamodeling. *Operations research*, 58(2):371–382, 2010.
- D. Azzimonti, J. Bect, C. Chevalier, and D. Ginsbourger. Quantifying uncertainties on excursion sets under a Gaussian random field prior. *SIAM/ASA Journal on Uncertainty Quantification*, 4(1):850–874, 2016.
- D. Azzimonti, D. Ginsbourger, C. Chevalier, J. Bect, and Y. Richet. Adaptive design of experiments for conservative estimation of excursion sets. *Technometrics*, pages 1–14, 2020.
- J. Bect, D. Ginsbourger, L. Li, V. Picheny, and E. Vazquez. Sequential design of computer experiments for the estimation of a probability of failure. *Statistics and Computing*, 22(3):773–793, 2012.
- B. J. Bichon, M. S. Eldred, L. P. Swiler, S. Mahadevan, and J. M. McFarland. Efficient global reliability analysis for nonlinear implicit performance functions. *AIAA Journal*, 46(10):2459–2468, 2008.
- M. Binois, J. Huang, R. B. Gramacy, and M. Ludkovski. Replication or exploration? Sequential design for stochastic simulation experiments. *Technometrics*, (just-accepted):1–43, 2018.
- D. Bolin and F. Lindgren. Excursion and contour uncertainty regions for latent Gaussian models. *Journal of the Royal Statistical Society: Series B (Statistical Methodology)*, 77(1):85–106, 2015.
- K. M. Bretthauer, A. Ross, and B. Shetty. Nonlinear integer programming for optimal allocation in stratified sampling. *European Journal of Operational Research*, 116(3):667–680, 1999.
- X. Chen and Q. Zhou. Sequential design strategies for mean response surface metamodeling via stochastic kriging with adaptive exploration and exploitation. *European Journal of Operational Research*, 262(2):575–585, 2017.
- C. Chevalier, D. Ginsbourger, J. Bect, and I. Molchanov. Estimating and quantifying uncertainties on level sets using the Vorob’ev expectation and deviation with Gaussian process models. In *mODa 10—Advances in Model-Oriented Design and Analysis*, pages 35–43. Springer, 2013.
- C. Chevalier, J. Bect, D. Ginsbourger, E. Vazquez, V. Picheny, and Y. Richet. Fast parallel kriging-based stepwise uncertainty reduction with application to the identification of an excursion set. *Technometrics*, 56(4):455–465, 2014a.
- C. Chevalier, D. Ginsbourger, and X. Emery. Corrected kriging update formulae for batch-sequential data assimilation. In *Mathematics of Planet Earth*, pages 119–122. Springer, 2014b.
- B. Echard, N. Gayton, and M. Lemaire. Kriging based Monte Carlo simulation to compute the probability of failure efficiently: AK-MCS method. *6emes Journées Nationales de Fiabilité, 24–26 mars, Toulouse, France*, 2010.

- R. Hu and M. Ludkovski. Sequential design for ranking response surfaces. *SIAM/ASA Journal on Uncertainty Quantification*, 5(1):212–239, 2017.
- H. Jalali, I. Van Nieuwenhuysse, and V. Picheny. Comparison of kriging-based algorithms for simulation optimization with heterogeneous noise. *European Journal of Operational Research*, 261(1): 279–301, 2017.
- D. R. Jones, M. Schonlau, and W. J. Welch. Efficient global optimization of expensive black-box functions. *Journal of Global Optimization*, 13(4):455–492, 1998.
- K. Kandasamy, G. Dasarathy, J. B. Oliva, J. Schneider, and B. Póczos. Gaussian process bandit optimisation with multi-fidelity evaluations. In *Advances in Neural Information Processing Systems*, pages 992–1000, 2016a.
- K. Kandasamy, G. Dasarathy, B. Poczos, and J. Schneider. The multi-fidelity multi-armed bandit. In *Advances in Neural Information Processing Systems*, pages 1777–1785, 2016b.
- K. Kandasamy, G. Dasarathy, J. Schneider, and B. Póczos. Multi-fidelity bayesian optimisation with continuous approximations. In *Proceedings of the 34th International Conference on Machine Learning-Volume 70*, pages 1799–1808. JMLR. org, 2017.
- A. Klein, S. Falkner, S. Bartels, P. Hennig, and F. Hutter. Fast Bayesian Optimization of Machine Learning Hyperparameters on Large Datasets. In A. Singh and J. Zhu, editors, *Proceedings of the 20th International Conference on Artificial Intelligence and Statistics*, volume 54 of *Proceedings of Machine Learning Research*, pages 528–536, Fort Lauderdale, FL, USA, 20–22 Apr 2017. PMLR. URL <http://proceedings.mlr.press/v54/klein17a.html>.
- J. Koehler, A. Puhalskii, and B. Simon. Estimating functions evaluated by simulation: A Bayesian/-analytic approach. *Annals of Applied Probability*, 8(4):1184–1215, 1998.
- L. Le Gratiet and J. Garnier. Asymptotic analysis of the learning curve for Gaussian process regression. *Journal of Machine Learning Research*, 98(3):407–433, 2015.
- M. Liu and J. Staum. Stochastic kriging for efficient nested simulation of expected shortfall. *Journal of Risk*, 12(3):3–27, 2010.
- M. Ludkovski. Kriging metamodels and experimental design for bermudan option pricing. *Journal of Computational Finance*, 22(1), 2018.
- M. Ludkovski and J. Risk. Sequential design and spatial modeling for portfolio tail risk measurement. *SIAM Journal on Financial Mathematics*, 9(4):1137–1174, 2018.
- X. Lyu, M. Binois, and M. Ludkovski. Evaluating Gaussian process metamodels and sequential designs for noisy level set estimation. *arXiv preprint arXiv:1807.06712*, 2018.
- M. McLeod, M. A. Osborne, and S. J. Roberts. Practical Bayesian optimization for variable cost objectives. *arXiv preprint arXiv:1703.04335*, 2017.
- V. Picheny, D. Ginsbourger, O. Roustant, R. T. Haftka, and N.-H. Kim. Adaptive designs of experiments for accurate approximation of a target region. *Journal of Mechanical Design*, 132(7):071008, 2010.
- M. Poloczek, J. Wang, and P. Frazier. Multi-information source optimization. In *Advances in Neural Information Processing Systems*, pages 4288–4298, 2017.

- P. Ranjan, D. Bingham, and G. Michailidis. Sequential experiment design for contour estimation from complex computer codes. *Technometrics*, 50(4):527–541, 2008.
- T. J. Santner, B. J. Williams, and W. I. Notz. *The Design and Analysis of Computer Experiments*. Springer Science & Business Media, 2013.
- N. Srinivas, A. Krause, S. M. Kakade, and M. W. Seeger. Information-theoretic regret bounds for Gaussian process optimization in the bandit setting. *IEEE Transactions on Information Theory*, 58(5):3250–3265, 2012.
- R. Stroh, S. Demeyer, N. Fischer, J. Bect, and E. Vazquez. Sequential design of experiments to estimate a probability of exceeding a threshold in a multi-fidelity stochastic simulator. *arXiv preprint arXiv:1707.08384*, 2017.
- K. Swersky, J. Snoek, and R. P. Adams. Multi-task Bayesian optimization. In *Advances in neural information processing systems*, pages 2004–2012, 2013.
- J. Vanhatalo, J. Riihimäki, J. Hartikainen, P. Jylänki, V. Tolvanen, and A. Vehtari. GPstuff: Bayesian modeling with Gaussian processes. *Journal of Machine Learning Research*, 14(Apr): 1175–1179, 2013.
- C. K. Williams and D. Barber. Bayesian classification with Gaussian processes. *IEEE Transactions on Pattern Analysis and Machine Intelligence*, 20(12):1342–1351, 1998.